ABSTRACT

COWELL, JASON M. Development of a Practical Fatigue Analysis Methodology for Life Prediction of Rotary-Wing Aircraft Components. (Under the direction of Dr. John S. Strenkowski.)

A practical fatigue analysis methodology was developed for predicting the life of rotary-wing aircraft components. The focus of this fatigue capability was two-fold. First, to gain insight into the current life prediction methodologies and their use, and second, to be able to predict the service life of aircraft components and determine if reworked parts are suitable for continued service. Commercially available software, ANSYS and Fe-safe, were utilized as the finite element and fatigue life prediction solvers, respectively.

It was demonstrated that the predicted fatigue life on aircraft components can be performed with reasonable accuracy and efficiency by utilizing commercially available software. This methodology was first demonstrated by investigating the predicted fatigue life of a flat plate with a centrally located hole under constant amplitude and variable amplitude loading. This approach was validated by comparing simulated life predictions using several stress-life and strain-life algorithms with previously published experimental data. In addition, an illustrative helicopter main gear drag beam was analyzed and the effect on fatigue life due to a reduction in the beam thickness was demonstrated.

This research had demonstrated that a fatigue life methodology can be successfully utilized to predict the service life of aircraft components in a practical manner and to determine if reworked parts are suitable for continued service.

DEVELOPMENT OF A PRACTICAL FATIGUE ANALYSIS METHODOLOGY FOR LIFE PREDICTION OF ROTARY-WING AIRCRAFT COMPONENTS

by

JASON MICHAEL COWELL

A thesis submitted to the Graduate Faculty of
North Carolina State University
in partial fulfillment of the
requirements for the Degree of
Master of Science

MECHANICAL ENGINEERING

Raleigh, North Carolina

2006

APPROVED BY:

Dr. Jerome J. Cuomo	Dr. Kara J. Peters

Dr. John S. Strenkowski
Chair of Advisory Committee

BIOGRAPHY

Jason Michael Cowell was born in Orange, California on December 22, 1974. He is the eldest son of Keith and Leilani Cowell, and has two brothers, Keith Cowell and Mark Cowell. He and his family moved to Harrisonburg, Virginia before his sophomore year of high school. After completing high school in Harrisonburg, he attended Virginia Tech where he earned a B.S in Mechanical Engineering and a B.S. in Math.

After graduation he married Melissa Sue Cerefice and began his engineering career working for Vishay Micro-Measurements as an Applications Engineer in Raleigh, NC. A little over a year later he left the engineering profession to work in the non-profit sector. He worked in the non-profit sector for two years until he was extended an invitation to return to academia to pursue a Master of Science in Mechanical Engineering from North Carolina State University. Working under the direction of Dr. John Strenkowski, research began in the area of fatigue analysis capabilities to predict the service life of aircraft components within the Aging Aircraft Community. Upon successful completion of the requirements for a Master of Science degree in Mechanical Engineering, he will begin employment with Northrop Grumman Electronic Systems.

ACKNOWLEDGEMENTS

I would like to sincerely thank my advisor Dr. John S. Strenkowski for giving me the opportunity to work under his guidance during my research. I would also like to thank the other two faculty members who served on my thesis committee, Dr. Jerome J. Cuomo and Dr. Kara J. Peters. I thank all the faculty and staff members of the Department of Mechanical Engineering, particularly Dr. Mohammed A. Zikry, Dr. Jeffery W. Eischen, and Dr. Carl F. Zorowski. I would also like to thank Mike Roedersheimer, Chris Draper, and Ian Mercer of Safe Technology Inc. and Mike Rife of ANSYS Inc. Additionally, I would like to thank Greg Sabin and Ken Workman at the Naval Air Depot at Cherry Point for their assistance in providing valuable information in regards to the fatigue problem.

Most importantly I would like to thank my wife for her continued support, encouragement and understanding. Although life got pretty hectic at times we made it through, you deserve as much credit for this work as I do.

TABLE OF CONTENTS

LIST OF TABLES

LIST OF FIGURES

1 INTRODUCTION

Currently, naval air depots are responsible for providing engineering support for maintaining several aircraft platforms, including the H-3, V-22, H-60 Skyhawk, and the AV-8. These aircraft are in service long beyond their design lifetime and due to the nature of the present day conflicts they are subjected to extreme environmental conditions e.g. desert sand and salt air. There is a need to predict the life of critical components for the timely scheduling of maintenance. Engineers are required to perform both static and fatigue analysis of structural components for all the supported aircraft platforms. At present, an adequate capability exists for static analysis. However, there is a need for a comprehensive fatigue and durability capability. This capability is needed to be able to predict the service life of aircraft components in a timely manner and determine if reworked parts are suitable for continued service. In the past, engineers at the air depots have relied on the original equipment manufactures (OEM's) for this fatigue analysis capability. Very often, the OEM's are not able to respond on a short-term basis and a premium is paid for outsourcing these analyses.

1.1 Main Objective

The main objective of this research is to develop a practical fatigue analysis methodology for life prediction of rotary-wing aircraft components. The focus of this fatigue capability is to be able to predict the service life of aircraft components and determine if reworked parts are suitable for continued service. The key to the success is not only to minimize the overall computational time of the numerical simulations, but also to gain an understanding of current fatigue capabilities and their use in maintenance scheduling.

Within the overall objective, several requirements must be met. The first requirement is to conduct a survey of commercially available fatigue software codes that could be used in an analytical fatigue and durability capability at naval air depots. The second requirement is to analyze a classical model, in order to validate the fatigue capability by gaining insight into the several life prediction techniques and to gain confidence in the results. The final requirement is to analyze and predict the service life of an illustrative complex aircraft component and determine if a reworked part is suitable for continued service.

1.2 Significance of the Research

In recent times, a new challenge has arisen in the aircraft structural integrity program within the naval fixed- and rotary-wing aircraft. A large number of these military aircraft are being operated beyond their design lives. For these aging aircraft, maintenance and repair costs have been steadily increasing due to a multitude of reasons, including but not limited to the presence of corrosion[1].

The predominant cause for the removal and replacement of an entire aircraft platform during the Cold War era was performance obsolescence. For this reason, aircraft platforms were removed and replaced much earlier than that which would have been determined by a fatigue life analysis. However, in today's military, aircraft are removed and replaced because of fatigue life and not because of performance requirements[2].

Current maintenance procedures for naval air-vehicles require the removal of corrosion when it is found with no formal mechanism for assessing the effect on fatigue life. This procedure is used because the sea environment in which naval aircraft operate is the most structurally hostile of environments and corrosion often acts as an accelerating agent for

crack propagation and it can promote crack initiation sites within the structure. Additionally, naval aircraft do not have the benefit of unscheduled inspections for fatigue cracking and thus crack initiation becomes the basis for life management. This is because naval aircraft are often deployed at sea for several months and maintenance hangars are not readily available.

Within the aging aircraft community a shift is beginning to emerge in which the design approach for rotorcraft is being questioned. Rotorcraft are typically designed using a safe-life philosophy. However, there is a growing interest in using the damage tolerance approach (DTA) because the FAA is considering implementing this design philosophy into the federal air regulations, FAR[3]. The increasing number of technical papers being published in this area reflects the growing interest in numerical simulations and the increase in computational techniques for predicting fatigue life. These papers document both research and experimental studies of numerous physical aspects of fatigue life prediction methodologies (mainly DTA) for critical aircraft components.

In fatigue analysis and the associated mathematical modeling, applying the strain-life approach for fatigue is vital for predicting time-to-crack initiation. By gaining an understanding of the different life prediction methodologies and their use, an analyst is better able to concentrate on specific simulation goals and life prediction approaches. There is a need for a fatigue and durability capability for timely scheduling of maintenance. This capability is needed to predict the service life of aircraft components in a timely manner and determine if reworked parts are suitable for continued service. Thus, the critical issue is not related to the design or redesign but the effects of maintenance in the field. Based on this

need, the research presented in this thesis will focus on the strain-life approach for life prediction using numerical simulation models.

1.3 Overview of Thesis

The following chapter presents a literature review of current trends in life prediction methodologies and their application to rotary-wing aircraft. The review also includes past research regarding experimental and analytical analyses of aircraft components. Additionally, the use of commercially available durability software for simulating crack initiation and propagation are described. Chapter 3 is an overview of fatigue life prediction methods, including the stress-life, strain-life, and fracture mechanics approaches for fatigue under constant amplitude loading. Chapter 4 broadens the life prediction methodologies by briefly describing the effects of variable amplitude loading. Chapter 5 describes a generic standard loading for aircraft components which is often used for comparison purposes, and Chapter 6 briefly describes multiaxial loading. In Chapter 7, an overview of fatigue life analysis based on finite element analysis is discussed, and Chapter 8 describes the modeling software used during numerical simulations. In Chapter 9, validations of the fatigue and durability software along with comparisons of the algorithms for both stress and strain life are conducted. The analysis and results of an illustrative aircraft component are given in Chapter 10. Conclusions and recommendations for future work are given in Chapter 11.

2 LITERATURE REVIEW

There have been a number of research publications in the open literature in the area of life prediction methodologies for aircraft components. Most of these publications have dealt with life prediction based on experimental techniques and computational algorithms for crack propagation. Analyses based on numerical simulations have increased in recent years due to the advances in both finite element and fatigue analysis software capabilities. Correlation between predicted and test results are now becoming very good, both for identifying hotspots (location of the initial crack site) and in predicting the actual fatigue life itself[4]. Recently the use of commercially available life prediction software has become a justifiable cost for improving the quality and efficiency of both design and test programs.

In general, previous studies have not accounted for the recent advances in fatigue analysis software capabilities and have thus typically been accomplished with in-house methodologies and software codes. More specifically, most studies have relied heavily on life prediction based on determining the crack growth time from an initial detectable crack size to some predetermined detrimental crack length. This is partially due to the fact that fatigue analysis is as much an art form as it is a science. During the past 30 years, the stress-analysis community has developed a large number of finite element codes to conduct linear and non-linear stress analyses of complex aircraft structural components[5]. Many of these codes contain special features to analyze crack propagation problems which are useful for determining the stress-intensity factor and its non-linear equivalent, the J-integral. Nevertheless, recent advances in multiaxial fatigue and its implementation into fatigue analysis software codes imply that fatigue analysis can be at least as accurate as other aspects

of engineering numerical simulations[6]. Thus, a life prediction analysis that incorporates time-to-crack initiation and its location would be beneficial for maintenance scheduling in predicting the service life of aircraft components.

Everett[7] refers to the work by Jacoby, in which one-third of the predicted lives of about 300 tests on several types of structures and materials were determined to be on the non-conservative side. Arden showed variations of 9 to 2,594 hours in predicted fatigue life of a hypothetical pitch link problem formulated by the American Helicopter Society (AHS). This brought into question as to whether the safe life approach (stress-life) was a reliable method for life prediction of rotary-wing aircraft.

Everett[7,8] participated in a round-robin study formulated by the AHS in the early 1990's that investigated a reliability-based fatigue methodology as well as the actual methodologies used to predict fatigue life. The test specimen was an isotropic flat plate with a central hole analyzed under both a uniaxial constant amplitude load and a uniaxial variable amplitude load. A S-N curve was developed along with the determination of the material properties for a strain-life approach to fatigue. The load spectrum used was that of a generic loading called Felix/28, which allowed for consistency within the participants of the round-robin study. Everett compared the predicted lives with the test lives for several different fatigue methodologies, including the stress-life, strain-life, damage tolerance (analysis based on an initial crack length, a_i, equal to 0.05 inches), and a damage tolerance approach based on small crack theory where the initial crack length was considered to be 0.0006 inches. He concluded that the DTA is extremely sensitive to the initial crack length and an analysis based on small crack theory was more accurate in determining life prediction to crack

initiation of a detectable crack. Additionally, he concluded that the safe life approaches predicted fatigue life with reasonable accuracy.

J.C. Newman[9,10,11,12] has been instrumental in the development of a fatigue life prediction methodology using small-crack theory. Numerous investigations have shown [10, 11] that very small cracks (0.00004 to 0.002 inches) have growth characteristics that are considerably different from large cracks (0.08 inches). Thus, this method utilizes a plasticity-induced crack closure model that treats fatigue as a crack-propagation process from a micro-defect (voids, inclusions, etc) to failure. Newman developed a crack growth life prediction program called FASTRAN[13] which accounts for retardation of plastically deformed material in the wake of a crack tip. Additionally, along with Forman and others, Newman developed the NASGRO equation used in NASA's crack growth life prediction program, NASGRO[14]. The NASGRO equation is also available in AFGROW[15], a crack growth prediction program developed by the U.S. Air Force.

Later work by Everett and Newman[16] assessed the effects of a machine-like scratch on the fatigue life of 4340 steel. It was shown both experimentally and by a FASTRAN analysis that a material with a machine-like scratch will experience a reduction in the endurance limit of the material. However, shot peening either a pristine material or a material containing a machine-like crack can increase the endurance limit.

Merati[17] conducted a study of nucleation and fatigue behavior of an aerospace aluminum alloy. It was noted that specimens under a high humidity environment experienced shorter fatigue lives than specimens operating in low humidity.

Hoffman and Hoffman raised the question "is the corrosion and fatigue research heading in the right direction to solve real and potential problems in aging aircraft?"[2]. In this paper they provided an overview of how the U.S. Navy validates and assesses service life with respect to structural integrity management of naval air vehicles. At the forefront of the naval policy is the preservation of flight safety throughout the entire service life-time and it is the cornerstone of all structural management plans. In this paper, the authors describe how naval aircraft are required to withstand randomly occurring fatigue loading without visible cracking during their design service life. Thus the main focus of reference [2] is that a safe-life approach for fatigue is acceptable in the design and analysis of all naval aircraft. This approach to fatigue differs significantly from the U.S. Air Force where the damage tolerant approach is used. Finally, the U.S. Navy currently defines failure as the formation of a 0.1 inch crack, which is derived from the strain-life approach and it is based on full-scale tests.

Adey and colleagues[18] describe an approach for predicting crack growth which combines the use of boundary element models (BEASY) with finite element models (NASTRAN). The approach removes the requirement of rebuilding FE models in order to capture stress concentrations and it enables the prediction of stress intensity factors for crack growth analysis. In this paper the authors suggest the need for crack initiation but state it can "normally be predicted based on the stress history which can be obtained from a suitable stress analysis".

Chu[19,20] describes the recent progress and application of multiaxial fatigue in component durability design within the ground vehicle industry. Typically, life predictions have been accomplished with a uniaxial fatigue life method. However, Chu notes that with

the advances in computing power and multiaxial fatigue algorithms, significant improvement in fatigue prediction accuracy has been achievable.

Several papers published by Draper[4,6,23,24,25,26] document the development of life prediction techniques based on finite element fatigue analysis. A commercially available computer code, fe-safe[27], developed by Draper has been used for life prediction of complex components under complex loadings. Excellent correlation has been achieved between numerical fatigue life simulations and experimental testing. In reference [6] a steel component from an aircraft control system was analyzed for time-to-crack initiation and compared with fatigue test results. Good correlation between the calculated life of 1631 repeats and the test life of 1650 repeats was achieved. In reference [27] a fatigue analysis was conducted on an end-yoke by Dana Corporation, Automotive Systems Group, USA. In this analysis the predicted location of the crack initiation site and the time-to-crack initiation collaborated well experimental results. However, principal stresses as determined by a finite element analysis resulted in the predicted critical area being different than was determined by the experimental results. Several other examples were outlined, including a steering knuckle from a car suspension[25]. The component consisted of three applied load histories at the tire contact patch and reasonable results were again achieved.

Of all the life prediction studies mentioned above, only the works reported by Draper[4,6,23,24,25,26] utilized commercially available software for life prediction based on time-to-crack initiation. There have been no other previous attempts to include the simulated effect of corrosion on the predicted fatigue life.

3 FATIGUE LIFE PREDICTION METHODS

Metal fatigue, which results in fatigue cracks, is the process of premature failure or damage of a component subjected to the repeated application of loads which individually would be too small to cause failure. Fatigue cracks usually initiate on the surface of the component on the microscopic scale and they are referred to as crack initiation or Stage I cracks. During the fatigue life, crack growth usually occurs on the macroscopic scale in the direction normal to the applied tensile stress, and it is referred to as crack propagation or Stage II. Finally, the component may fail due to fracture.

Earlier fatigue theories analyzed the entire fatigue life of a component as a single entity. However, modern fatigue theories analyze each of the three stages of fatigue life separately. This is typically accomplished by splitting the fatigue life into two periods: the crack initiation period followed by the crack propagation or growth period. It is very difficult if not impossible to define the transition from initiation to propagation of crack growth due to the variability in crack length.

3.1 Introduction to the Safe-Life and Damage Tolerance Methodologies

There are three primary fatigue analysis methods, the stress-life approach (S-N), the strain-life approach (ε-N) and the fracture mechanics or damage-tolerance approach. All three analysis methods have their own region of application, but with some degree of overlap. Therefore, it is advantageous to gain an understanding of all three methods in order to allow the engineer to have the insight as to which method or methods are most suitable for a given fatigue problem.

Currently, none of the methods are accurate enough to completely eliminate the need for testing. In addition, the precision of each of the techniques for predicting fatigue life is a function of how well the input variables are defined. Typically, the particular method chosen for analysis is based on its level of acceptance and the confidence that the designer/analyst has in the method. The stress-life approach was introduced about 150 years ago, the strain-life approach about 40 years ago, and the damage-tolerance approach, which is based on Linear-Elastic Fracture Mechanics (LEFM), was introduced about 30 years ago. The level of acceptance of the stress-life approach is widespread and this technique is usually taught at the undergraduate level thus, it requires only an understanding of elastic stress analysis. Both the strain-life and damage-tolerance approaches require increased levels of technical background in elastic-plastic stress-strain properties and fracture mechanics, respectively[28]. However, there is no general fatigue analysis method for all applications; each technique has its strengths and weaknesses and the selection must be based on material, load history, operating environments such as corrosion, surface finish, and residual stresses and fretting between adjacent surfaces.

The remaining sections of Chapter 3 provide a basic description of the three primary fatigue analysis methods. A more extensive description of the safe-life and damage-tolerance methodologies can be found in references [28], [29], and [30], with reference [30] dealing primarily with LEFM.

3.2 Stress-Life Approach

3.2.1 Introduction

The stress-life approach was first introduced by Wohler in the 1860's and presents a means of determining the fatigue life of a smooth (unnotched) specimen subjected to an applied alternating stress. This empirical method is best suited for high cycle fatigue (HCF) and introduces the concept of an endurance or fatigue limit. This traditional approach was developed in its present form by 1955 and it is based on the nominal stresses in the region of the component being analyzed.

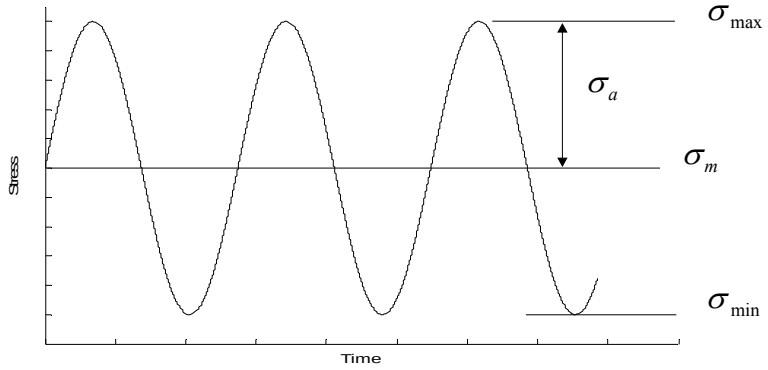

Figure 3.1 – Constant Amplitude Cycle Terminology

Several parameters must first be defined in order to discuss the stress-based approach for fatigue. These parameters are shown schematically in Figure 3.1, which shows a sinusoidal waveform of a fatigue cycle. The stress range, $\Delta\sigma$, the stress amplitude, σ_a, and the mean stress, σ_m, are defined as:

$$\Delta\sigma = \sigma_{max} - \sigma_{min}, \qquad \sigma_a = \frac{\Delta\sigma}{2}, \qquad \sigma_m = \frac{\sigma_{max} + \sigma_{min}}{2} \tag{1}$$

Additionally, ratios of the above parameters are often used and defined by:

$$R = \frac{\sigma_{\min}}{\sigma_{\max}}, \qquad A = \frac{\sigma_a}{\sigma_m} \tag{2}$$

Where R and A are the stress and amplitude ratios, respectively. With the stress ratio defined in this manner, fully reversed loading occurs when R = -1, zero-to-tension fatigue occurs when R = 0, and static loading occurs when R = 1.

3.2.2 S-N Diagrams

The basis of the stress-based method is the stress-life curve, also called the S-N diagram, where the amplitude of stress (σ_a) or nominal stress (S_a) is plotted versus the number of cycles to failure, N_f. The number of cycles to failure is usually plotted on a logarithmic scale since the cycle numbers change rapidly with the stress magnitude. Two distinct types of S-N behavior are represented schematically in Figure 3.2. As these figures imply, higher stress magnitudes result in reducing the number of cycles that the material is capable of sustaining before failure. Additionally, some ferrous materials, such as plain-carbon and low-alloy steels, exhibit a distinct endurance limit (S_e), where the S-N curve becomes flat and asymptotically approaches the stress amplitude of S_e. However, for materials such as aluminum and copper alloys, the S-N curve does not appear to approach an asymptote. Thus the fatigue limit is specified by the fatigue strength and defined by the stress level at which failure will occur for a specified number of cycles, typically defined between 10^7 and 10^8 cycles. The endurance limit for most ferrous materials is often related to the ultimate strength (S_u) of the material.

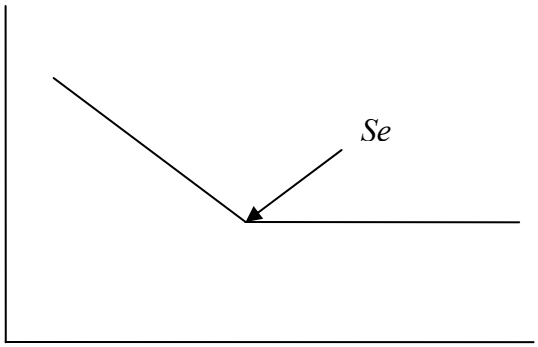

Cycles to Failure, N_f
(log scale)
(a)

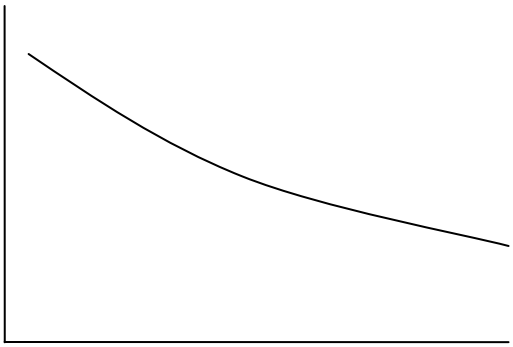

Cycles to Failure, N_f
(log scale)
(b)

Figure 3.2 – S-N Curves for (a) Material Displaying a Fatigue Limit and (b) Material Not Displaying a Fatigue Limit

The data points of the S-N curve are determined experimentally from an unnotched specimen under constant amplitude loading with a zero mean stress, or at some specific nonzero mean stress, σ_m. The test is repeated at increasingly higher stress levels equating to lower cycles to failure. During the development of S-N curves it is not uncommon to observe an order magnitude uncertainty in statistical scatter of the test data. The resulting S-N curve consists of averaging the number of life cycles for each applied stress level. A linear relationship of the averaged curve is commonly observed on a log-log plot with the mathematical representation of the curve obtained by the following equation:

$$\frac{\Delta\sigma}{2} = \sigma_a = \sigma_f^{'}\left(2N_f\right)^b \tag{3}$$

Where $\sigma_f^{'}$ is the fatigue strength coefficient and is often approximately equal to the true fracture strength σ_f and b is known as the fatigue strength exponent or Basquin exponent.

Both σ_f and b are fatigue properties of the material. Lastly, $2N_f$ or half-cycles is the number of reversals to failure and N_f is the number of cycles.

3.2.3 Mean Stress Effects

Thus far, the empirical description of the fatigue life pertains to fully reversed fatigue loads where the mean stress of the fatigue cycle, $\sigma_{m,}$ is equal to zero. However, this is not necessarily representative of many applications where in fact the mean stress may not be equal to zero. The fatigue behavior of engineering materials is known to be greatly influenced by the mean level, where typically a mean tensile stress is more detrimental than a mean compressive stress. It has been observed that increasing the mean stress level decreases the fatigue life [4].

Mean stress effects in fatigue can be represented by constant-life diagrams, as shown in Figure 3.3. Stresses falling above the possible failure criteria lines result in failure. The most well known failure models are the Gerber line and the Modified Goodman line which are best used for fracture criteria, and the Soderberg line which is best used for yield criteria. The failure models are described by the following equations:

Gerber (1874):
$$\frac{\sigma_a}{S_e} + \left(\frac{\sigma_m}{S_u}\right)^2 = 1 \tag{4}$$

Modified Goodman (1899):
$$\frac{\sigma_a}{S_e} + \frac{\sigma_m}{S_u} = 1 \tag{5}$$

Soderberg (1939):
$$\frac{\sigma_a}{S_e} + \frac{\sigma_m}{S_y} = 1 \tag{6}$$

Morrow (1960): $$\frac{\sigma_a}{S_e} + \frac{\sigma_m}{\sigma_f} = 1 \qquad (7)$$

Where:

S_y = the yield strength.

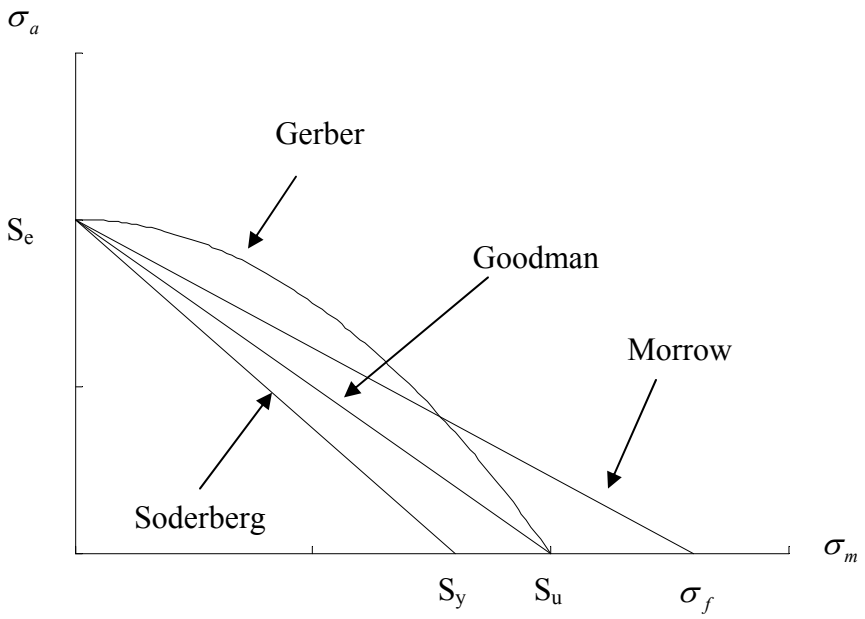

Figure 3.3 – Comparison of Constant Life Curves

Some general observations can be made on the failure criteria models when discussing cases of tensile mean stresses. The Gerber model is generally appropriate for ductile alloys but does not distinguish between tensile and compressive mean stresses. The Modified Goodman model is best suited for brittle metals. It is generally conservative for ductile alloys and it is generally non-conservative for compressive mean stresses. The Soderberg model is seldom used since this method is very conservative for most alloys.

While the Basquin model, given by equation 3, is only valid for a mean stress of zero, a more general equation that accounts for a nonzero mean stress was developed by Morrow in 1968. This modified Basquin model is described by the following equation:

$$\sigma_a = \left(\sigma_f^{'} - \sigma_m\right)\left(2N_f\right)^b \tag{8}$$

3.2.4 Modifying Factors

Several modifying factors are usually considered when using the stress-based approach for fatigue analysis of a smooth unnotched test specimen. Years of testing of the effects of various factors such as: surface finish and treatments (k_a), size (k_b), loading (k_c), temperature (k_d), and other miscellaneous effects (k_e) such as the environment have been quantified as modification factors that result in a modified endurance limit often denoted as $S_e^{'}$. The modified endurance limit tends to be conservative with a correction for the remainder of the S-N curve not clearly defined. The modified endurance limit has the form:

$$S_e^{'} = k_a k_b k_c k_d k_e S_e \tag{9}$$

The endurance limit will typically be reduced by the tensile mean stress, large section size, rough surface finish, chrome and nickel plating, decarburization (due to forging and hot rolling) and severe grinding. The endurance limit will typically be increased by modifying factors such as nitriding, carburization, shot peening, cold rolling, and induction hardening [31].

3.2.5 Notches

The discussion of the stress-based approach of fatigue has focused on nominally smooth-surfaced solid test specimens. However, almost all machine components and structural members invariably contain geometric or micro-structural discontinuities such as holes, fillets, grooves, and keyways. These discontinuities, or stress concentrations, cause the stress to be locally elevated, thus having a strong effect on how fatigue cracks nucleate and propagate [29].

The elastic stress concentration factor K_t relates the local stress ahead of the notch tip to the far-field loading and is defined by the ratio of the maximum local stress at the discontinuity, $\sigma_{max,}$ to the nominal stress of the member, S.

$$K_t = \frac{\sigma_{\max}}{S} \tag{10}$$

This theoretical stress concentration factor is a function of the component geometry and loading and is available in many handbooks with the most popular and well used being that of Peterson [32].

Under fatigue loading conditions the effect of notches are accounted for by the fatigue notch factor K_f, which unlike K_t, is also dependent on material type.

$$K_f = \frac{S_e^{(unnotched)}}{S_e^{(notched)}} \tag{11}$$

To account for these additional effects, the so-called notch sensitivity factor, q, was developed and is defined as

$$q = \frac{K_f - 1}{K_t - 1} \qquad q = \frac{1}{\left(1 + \frac{\alpha}{\rho}\right)} \tag{12}$$

Where **r** is the notch-root radius and **a** is a constant dependent on the strength and ductility of the material. The parameter q varies from zero for no notch effect ($K_f = 1$) to unity for the full effect predicted by elasticity theory ($K_f = K_t$).

3.2.6 Concluding Remarks

The S-N method is quite simple and can be used in almost any situation to obtain an initial rough estimate of the fatigue life. The method works well in applications of constant amplitude loading and designs involving long fatigue lives (effects due to variable amplitude loading will be discussed in a latter section). There are many existing S-N and test data readily available. However, this method is completely empirical and it derives from tensile tests of materials in the intermediate to long life region. Additionally, this method ignores plastic strains, which are critical for short fatigue lives, and this method is often dependent on geometry.

3.3 Strain-Life Approach

3.3.1 Introduction

The strain-life approach was initially developed independently by Coffin and Manson in the 1950's. This method assumes that in many practical applications the engineering component response of the material will undergo plastic deformation, particularly at locations with stress concentrations. The strain-based method accounts for situations of local

yielding, which is often the case for low cycle fatigue (LCF) of ductile metals but may also be applied during high cycle fatigue (HCF) when there is little plasticity. Thus the strain-life approach differs significantly from the stress-life approach, as described earlier, which emphasizes nominal stresses and elastic stress concentration factors with empirical modifications.

Equivalent fatigue life (as well as fatigue damage which is discussed in Section 4.2) is assumed to occur in the material of an engineering component at the notch root and a smooth test specimen. This is due to the constraint imposed by the elastically stressed material surrounding the plastic zone when both are subjected to identical load histories as shown in Figure 3.4.

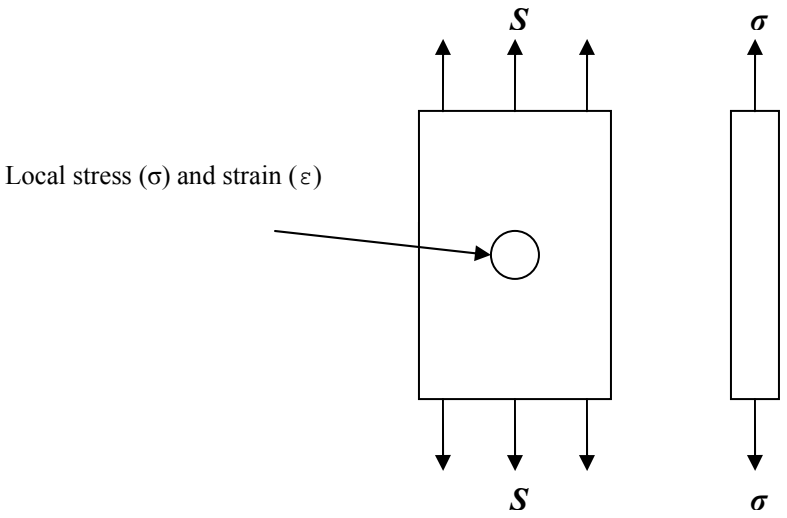

Figure 3.4 – Strain Based Approach for Fatigue of a Notched and Smooth Specimen

3.3.2 True Stress and Strain

A monotonic tensile test of a smooth cylindrical test specimen, which is obtained from a single load application, is typically used to determine the engineering stress and strain behavior of a material. However, in analyzing the results of tensile tests, the test specimen not only exhibits an increase in length but the specimen will also undergo a reduction in diameter. Therefore, the true stress is defined as the applied load P divided by the actual cross-sectional area A, rather than the original area A_o.

$$\sigma_{true} = \frac{P}{A} \tag{13}$$

Similarly, true strain is calculated from small increments in the instantaneous length and defined by

$$\varepsilon_{true} = \ln\left(\frac{l}{l_o}\right) \tag{14}$$

It must be noted that the simple relationships given by Equations (13) and (14) are only valid up to necking. Once necking has occurred, the stress is not uniformly distributed across the section.

The difference between engineering and the true stress-strain response of a ductile material is shown in Figure 3.5. The true stress-strain curve consists of an elastic portion (ε_e) which is recovered when the load is removed and a plastic portion (ε_p) which is not recovered. They are both defined by the following relationships:

$$\varepsilon_e = \left(\frac{\sigma}{E}\right) \qquad \varepsilon_p = \left(\frac{\sigma}{K}\right)^{\frac{1}{n}} \tag{15}$$

Where:

E = the elastic modulus

K = strain hardening coefficient

n = strain hardening exponent derived from monotonic stress-strain data.

Ramberg and Osgood proposed that the total strain can be defined by the summation of the elastic and plastic strains.

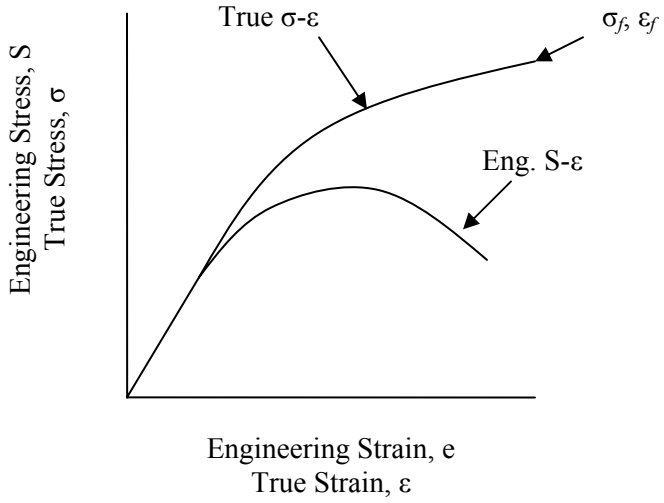

Figure 3.5 – Comparison of Engineering and True Stress-Strain

3.3.3 Fatigue Life Relationships

If a test specimen is loaded in tension and then compression with yielding occurring at each load application of the half-cycle, the Bauschinger effect as seen in Figure 3.6 is

observed. If the test specimen is then loaded again in tension, completing one full cycle, the closed loop is known as a hysteresis loop as shown in Figure 3.7.

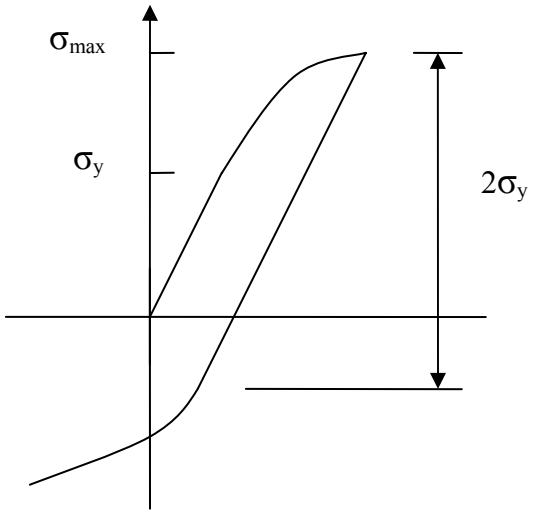

Figure 3.6 – Bauschinger Effect

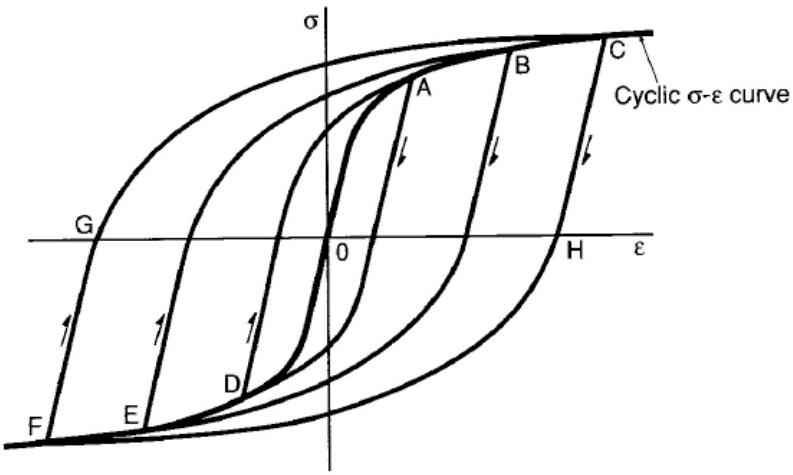

Figure 3.7 – Hysteresis Loop [29]

Cyclic stress-strain curves where a line from the origin passes through the tips of several loops, such as O-A-B-C in Figure 3.7 are used for assessing the durability of components and structures subjected to repeated loading, and are similar to monotonic stress-strain curves obtained during static load tests. The total width of loop C-H-F-G is $\Delta\varepsilon$ and the total height of the loop is $\Delta\sigma$, or total strain and stress ranges, respectively. The area within the loop represents a measure of the work done on the material due to plastic deformation. Thus, the total strain is the sum of the elastic and plastic strain ranges.

$$\Delta\varepsilon = \Delta\varepsilon_e + \Delta\varepsilon_p \tag{16}$$

The response of a material subjected to a cyclic inelastic loading (that is at each load application yielding occurs) is in the form of a hysteresis loop and represents the true stress versus true strain and is defined by the following equation:

$$\Delta\varepsilon = \frac{\Delta\sigma}{E} + 2\left(\frac{\Delta\sigma}{2K'}\right)^{\frac{1}{n'}} \tag{17}$$

Where primes are used to specify that the constants for the plastic term are from cyclic rather than monotonic stress-strain data and Δ represents the stress and strain ranges relative to coordinate axes at either loop tip. In addition, the stress-strain path for the hysteresis loops typically has the same shape as the cyclic stress-strain curve (Ramber-Osgood equation from cyclic stress-strain data) except for the addition of a scale factor of two.

3.3.4 Strain-Life Curves

As with the stress-life approach, if several specimens are tested under different constant amplitude loads with a zero mean stress, test lives of the elastic and plastic regions

can be plotted on the basis of the true stress amplitude. By dividing both sides of Equation (3) (Basquin equation) by the elastic modulus E, the elastic strains commonly result in a linear relationship with a shallow slope when plotted on a log-log plot.

$$\frac{\Delta\varepsilon_e}{2} = \frac{\Delta\sigma}{2E} = \frac{\sigma_f^{'}}{E}\left(2N_f\right)^b \tag{18}$$

The Coffin-Manson equation showed that the relationship between plastic strain amplitude and endurance also commonly results in a linear relationship when plotted on a log-log plot, but with a much steeper slope.

$$\frac{\Delta\varepsilon_p}{2} = \varepsilon_f^{'}\left(2N_f\right)^c \tag{19}$$

Combining equations 18 and 19 results in the basis of the strain-life method, which relates the total strain amplitude to the fatigue life and is given by the following relationship [29]

$$\frac{\Delta\varepsilon}{2} = \underbrace{\frac{\sigma_f^{'}}{E}\left(2N_f\right)^b}_{elastic} + \underbrace{\varepsilon_f^{'}\left(2N_f\right)^c}_{plastic} \tag{20}$$

Where:

$\varepsilon_f^{'}$ = the fatigue ductility coefficient

c = the fatigue ductility exponent

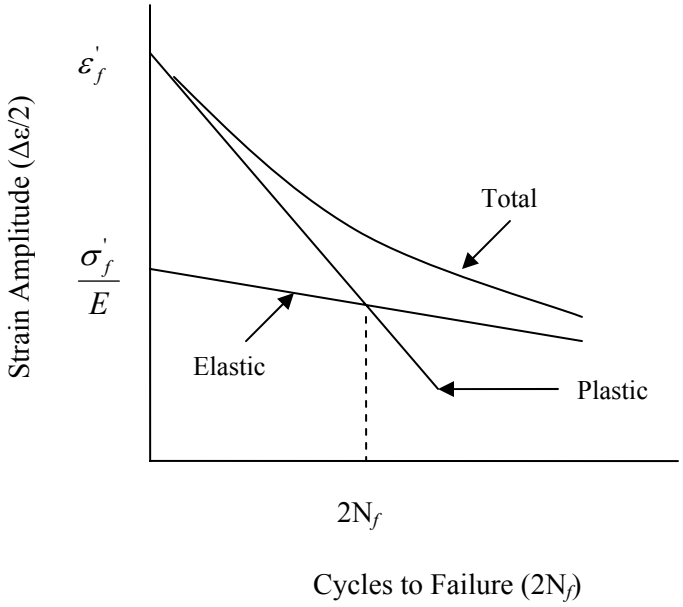

Figure 3.8 – Elastic, Plastic, and Total Strain vs. Life Curves

3.3.5 Mean Stress Effects

For the most part, the effect of mean strain is negligible on the fatigue life of a component. However, mean stress may have a significant effect on the fatigue life, predominantly at longer lives. Mean stress effects can either increase the fatigue life under compressive loads or decrease the fatigue life under tensile loads. A number of modifications to the strain-life equation, Equation (20), that incorporate the effect of mean stress are currently being used. However, no consensus exists on which approach is best [4].

Morrow suggested that the mean stress effect could be accounted for by modifying the elastic term in the strain-life equation by subtracting the mean stress, σ_m. The strain-live equation then becomes

$$\frac{\Delta\varepsilon}{2} = \frac{\sigma_f' - \sigma_m}{E}\left(2N_f\right)^b + \varepsilon_f'\left(2N_f'\right)^c \tag{21}$$

Another approach to account for mean stress effects was proposed by Smith, Watson, and Topper (SWT) [33]. They suggested that fatigue life was the product of strain amplitude and maximum stress in the cycle. Recalling Equation (3) at zero mean stress i.e. (σ_{max} = $\Delta\sigma/2$) and multiplying the strain-life equation by this term, results in

$$\frac{\Delta\varepsilon}{2}\sigma_{\max} = \frac{\left(\sigma_f^{'}\right)^2}{E}\left(2N_f\right)^{2b} + \sigma_f^{'}\varepsilon_f^{'}\left(2N_f\right)^{b+c} \tag{22}$$

3.3.6 Stress Concentrations

Stress concentration factors as described previously are equal to strain concentration factors when elastic deformation occurs at the tip of the notch. However, once the material yields at the notch tip (local yielding) the local stress (σ) and local strain (ε) are no longer linearly related. Thus, concentration factors estimated by elastic analysis alone become invalid. At this point it becomes necessary to define separate stress and strain concentration factors, where *S* and *e* are the nominal stress and strain, respectively [29].

$$K_\sigma = \frac{\sigma}{S} \qquad K_\varepsilon = \frac{\varepsilon}{e} \tag{23}$$

3.3.7 Nueber's Rule

The strain-life method accounts for notch-root plasticity by requiring that the notch root stresses and strains be known. These are typically determined either experimentally by strain gage measurements or through numerical analysis such as finite elements. It is often advantageous to analyze an engineering component using linear elastic finite element analysis as opposed to a nonlinear elastic-plastic analysis. Although nonlinear elastic-plastic

numerical analysis is sometimes necessary i.e. during fully plastic yielding, Neuber's rule is a method used for estimating notch stresses and strains from a linear elastic model. Thus, it is essentially used as a correction factor. Neuber's rule is defined by

$$K_t = \sqrt{K_\sigma K_\varepsilon} \tag{24}$$

This can be rearranged to directly convert stresses from an elastic finite element analysis (σ^e, ε^e representing elastic stress-strain) into elastic-plastic stress-strain (σ, ε representing elastic-plastic stress-strain). It is used with the cyclic and hysteresis stress-stain curves and the relationship can be seen in Figure 3.9.

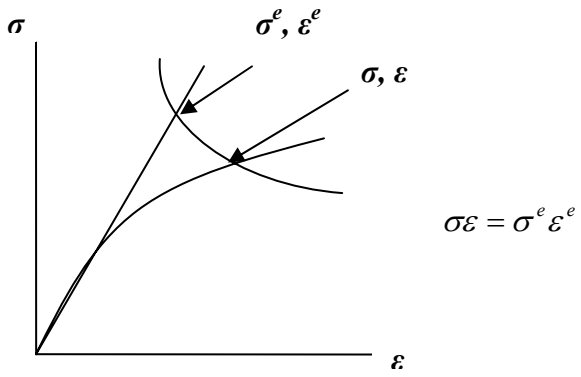

Figure 3.9 – Neuber's Rule

Assuming fully plastic yielding does not occur; Neuber's rule for local yielding is defined by the following equation,

$$\underbrace{\sigma\varepsilon}_{\substack{notch\\response}} = \underbrace{\frac{(K_t S)^2}{E}}_{\substack{applied\\load}} \tag{25}$$

3.3.8 Concluding Remarks

The strain-life method takes into account the actual stress-strain response of the material and thus accounts for localized plasticity. This method is suitable for estimating both long and short lives and it is well-suited for handling variable amplitude loading (discussed in Chapter 4). It can handle complicated geometries such as notches and it takes into account the mean stress correction. This method involves a relatively complicated analysis by hand but it is ideally suited with the use of computer analysis. The strain-life approach is attractive for practical reasons since strains can be measured using strain gages and it is well-suited for application with finite element analysis (FEA). However, this method along with the stress-based approach does not include an analysis of crack growth. The analysis of crack growth is accomplished through the use of fracture mechanics.

3.4 Fracture Mechanics Approach

3.4.1 Introduction

Modern theories of fracture mechanics as an engineering discipline were introduced in the mid 1950s by George R. Irwin. This approach for life prediction is used to determine the life of a component during crack propagation, with the total life of a component equating to the sum of the crack initiation and propagation. The fracture mechanics approach requires that an initial crack size be known or assumed. In addition to the crack itself, other types of flaws (voids, inclusions, casting defects, etc.) that are crack-like in form may develop into cracks. This life prediction analysis type is referred to as the Damage Tolerance Approach (DTA) for fatigue.

3.4.1.1 Linear Elastic Fracture Mechanics

In ductile materials, large plastic deformations occur in the vicinity of a crack tip since materials plastically deform as the yield stress is exceeded. As long as this region of plasticity remains small in relation to the overall dimensions of the crack and cracked body, the linear elastic fracture mechanics (LEFM) approach is valid. Thus the LEFM is a mature field in which the material is assumed to behave in a linear-elastic manner as defined by Hooke's Law.

3.4.2 Loading Modes

A cracked body can be generally loaded in any one or a combination of the three modes of loading as shown in Figure 3.10. Mode I is the normal or opening mode, Mode II is the sliding or in-plane shear mode, and Mode III is the tearing or anti-plane shear mode. The following discussion deals with crack propagation due to Mode I since it is the most important for practical analysis within most engineering applications.

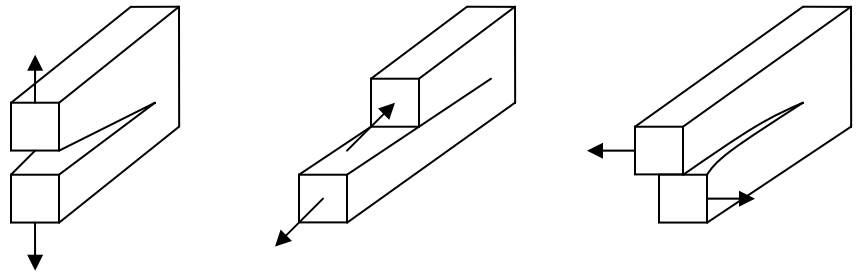

Figure 3.10 – Three Basic Independent Modes of Crack Deformation

3.4.3 Stress Intensity Factor

For a semi-infinite through-thickness crack of size *a*, in an infinite plate of an isotropic and homogeneous solid loaded in Mode I, the stress distribution near the crack tip is of the general form

$$\theta_{ij} = \frac{K_I}{\sqrt{2\pi r}} f_{ij}(\theta) + \ldots \tag{26}$$

Where:

θ_{ij} = the local stresses acting on an element *dxdy* at a distance r from the crack tip and at an angle theta from the crack plane

$f_{ij}(\theta)$ = known functions of theta

The stress intensity factor, K_I where I denotes mode I loading, defines the magnitude of the local stresses around the crack tip.

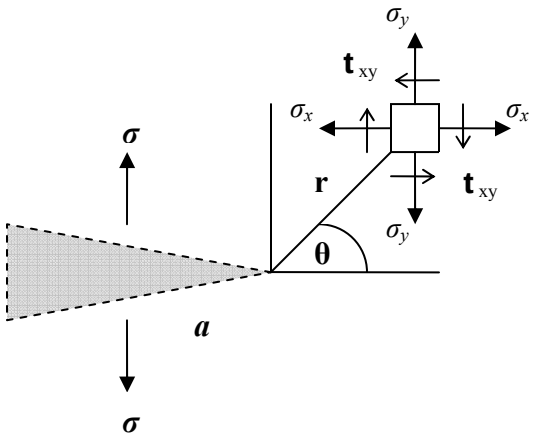

Figure 3.11 – Location of Local Stress near a Crack Tip

The stress intensity factor is affected by crack size and shape, loading, and geometry. For Mode I it has the general form,

$$K_I = \sigma\sqrt{\pi a}F(g) \tag{27}$$

Where:

σ	=	the applied far-field stress
a	=	the crack length
F	=	a dimensionless correction factor that depends on geometry and loading

Solutions for stress intensity factors for a wide variety of problems have been obtained and published in several readily available handbooks [30].

3.4.4 Fracture Toughness

The value of the stress intensity factor, K_I, at fracture is called the fracture toughness and denoted K_c. Thus fracture occurs when K_I equals K_c regardless of the shape of the body or the size of the crack.

As discussed earlier, stresses are very high at the crack tip. Therefore, a large transverse strain should develop in the plastic zone. However, the material surrounding the plastic zone is at a much lower stress, which constrains the crack tip from contracting. This deters transverse strains from developing but the material is subjected to transverse stress. It must be noted that transverse stress will only develop if the material is sufficiently thick i.e. a plain strain condition. In a thin body, the out of plane stresses (σ_z) are zero equating to a plane stress condition [30].

The behavior of cracks is different in plane strain and plane stress conditions which implies that the fracture toughness for both conditions is also different. This means fracture toughness is dependent on the thickness of the material [30]. For plane strain conditions the

toughness is called the plane strain fracture toughness and usually denoted K_{Ic} for mode I loading.

3.4.5 Fatigue Crack Growth

It has been found that the majority of fatigue life occurs during the propagation of a crack. Therefore, fracture mechanics principles enable the prediction of the number of cycles for a crack to grow to some specified length or to final failure of the component.

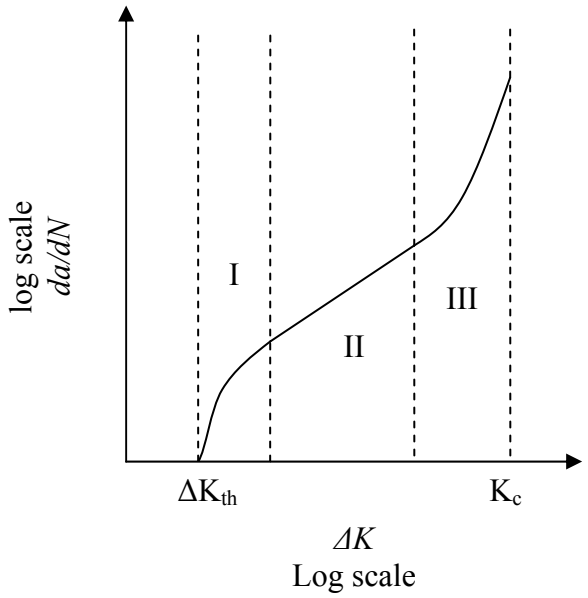

Figure 3.12 – Idealized Regions of the Crack Growth Rate Curve

Crack growth behavior for constant amplitude loading can be described by the relationship between cyclic crack growth rate *da/dN* and the stress intensity range ΔK. Values of log *da/dN* versus values of log ΔK can be plotted for a given crack length as shown in Figure 3.12. This curve may be divided into three regions. At low growth rates, Region I,

the curve appears to approach a vertical asymptote in which the cracking behavior is associated with ΔK_{th} called the fatigue crack growth threshold. It is in this region that crack growth does not ordinarily occur. At higher growth rates, Region III, unstable crack growth occurs just prior to final failure. Most of the current applications of LEFM to describe crack growth occur in Region II. It is at these intermediate values of ΔK, that a straight line on a log-log plot is often observed. A relationship representing this line was developed by P. C. Paris in the early 1960's and is given by

$$\frac{da}{dN} = C(\Delta K)^m \tag{28}$$

Where:

C = material constant

m = material constant and slope of the log-log plot

ΔK = the stress intensity range K_{max} - K_{min}.

The crack growth life, in terms of cycles to failure under constant amplitude loading, may be calculated by integrating the Paris equation over the interval a_i (the initial crack length) to a_f (the final or critical crack length).

$$N_f = \int_{a_i}^{a_f} \frac{da}{C(\Delta K)^m} \tag{29}$$

3.4.6 Mean Stress Effects

As with both the stress-life and strain-life approaches to fatigue, mean stresses can have a significant effect on the fatigue life of a component. An increase in the R-ratio of the cyclic loading causes growth rates for a given ΔK to be larger. Various empirical

relationships characterizing the effect of R on *da/dN* vs. *ΔK* curves will now briefly be discussed. One of the most widely used methods is based on applying the Walker relationship which is defined by the following equation

$$\frac{da}{dN} = \frac{C(\Delta K_I)^m}{(1-R)^n} \tag{30}$$

Where:

n = material constant

Another proposed method to include R effects is that of Forman and is defined by the following equation.

$$\frac{da}{dN} = \frac{C(\Delta K)^m}{(1-R)K_c - \Delta K} \tag{31}$$

These models do not account for any micro-structural or environmental effects and need to be further modified.

3.4.7 Crack Size Limitations

The practice of characterizing the growth of fatigue cracks on the basis of fracture mechanics typically relies on components containing long cracks or flaws with an initial length of about 0.05 inches [7]. However, if a crack is sufficiently small and thus interacts with the microstructure of the material it can have dramatic effects on crack growth behavior. The growth of small cracks, when described by LEFM, tends to grow faster than estimated from the usual *da/dN* vs. *ΔK* curves from test specimens with long cracks. This is illustrated in Figure 3.13.

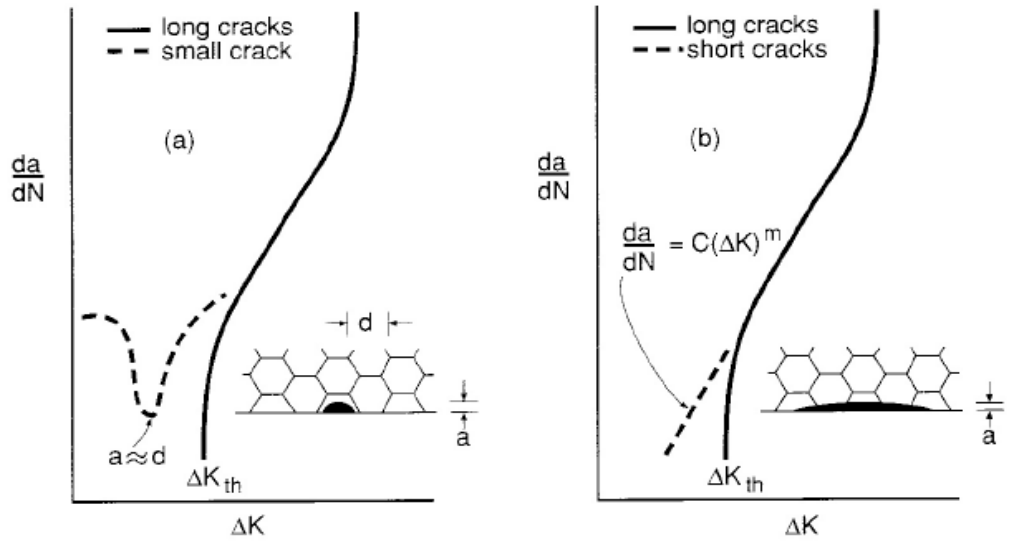

Figure 3.13 – Behavior of Small and Short Cracks on a Microstructural Scale [29]

Small cracks are defined when all of its dimensions are comparable to the micro-structural dimensions, such as grain size, of the material. However, short cracks have one dimension that is large compared to the microstructure [29].

In the early 1970's, Elber developed the theory of crack closure. He observed that the surfaces of fatigue cracks close as a result of crack-tip plasticity and thus cannot propagate until the applied stress exceeds the stress necessary to fully open the crack faces. Thus, from crack closure considerations, ΔK in Equation (28) is replaced by an effective stress intensity factor range, ΔK_{eff}, which is smaller than ΔK and defined as

$$\Delta K_{eff} = K_{\max} - K_{open} \tag{32}$$

$$\Delta K_{eff} = \left(S_{\max} - S_o\right)\sqrt{\pi a}F\left(g\right) \tag{33}$$

Where S_o is the crack-opening stress as calculated from the analytical closure model developed by Newman[9,14]. To calculate the crack growth rate due to the effects of small cracks, Equation (28) becomes

$$\frac{da}{dN} = C\left[\left(S_{\max} - S_o\right)\sqrt{\pi a}F(g)\right]^m \tag{34}$$

Therefore, to calculate the total life of a component using the fracture mechanics approach a modified damage tolerance approach is used which incorporates the effects of small cracks. This approach is referred to as the total life analysis (TLA) and is described by Everett in reference [7].

3.4.8 Crack Propagation for Complex Components

Standard references are readily available giving values of the shape parameter or correction factor, *F*, of many simple classical shapes for use with the Paris, Walker, or Forman equations. However, in practice many components are of a complex shape and thus the fatigue crack growth equations with the shape parameter are not valid. This results in the need for a full FEA or boundary element analysis allowing for stress redistribution as the crack propagates. Another problem with complex components is defining the effective remote stress [4].

3.4.9 Concluding Remarks

The LEFM approach is the only method that deals directly with crack growth and provides a method to characterize the failure due to fracture. Crack growth rates can be incorporated with nondestructive inspection techniques to find the apparent safe life of

cracked components and it is well-suited for determining the life of a component with notches. Limitations of the method include crack initiation and it can be difficult to estimate the initial crack size. However, advances in a crack-closure based model along with small-crack growth characteristics to predict total fatigue life will continue the need for research.

4 FATIGUE UNDER VARIABLE AMPLITUDE LOADING

Up to this point most of the discussion about fatigue has dealt with constant amplitude loading. Constant amplitude fatigue loading is defined as fatigue under cyclic loading with constant amplitude and a constant mean load. However, engineering components are usually subjected to variable amplitude loading which can be defined by complex loading histories of varying cyclic stress amplitudes, mean stresses and loading frequencies.

4.1 Cycle Counting

For highly irregular variations of load with time, as shown in Figure 4.1, it is not obvious how individual events should be isolated and defined as cycles. To predict the life of a component subjected to a variable load history it is necessary to reduce the complex history into a number of events represented as a repeating block of load cycles. Real structures rarely experience constant amplitude loading; however, fatigue lives are determined from constant amplitude tests. The most widely used approach for reducing a complex load history is a technique referred to as cycle counting. This fairly simple procedure was developed by Prof. T. Endo and his colleagues in Japan around 1968 and is referred to as Rainflow Cycle Counting. An in-depth discussion on cycle counting will not be discussed in this paper. It is suggested the reader review the cycle counting method published by Downing and Socie [34] and/or the "*SAE Fatigue Design Handbook*" [35].

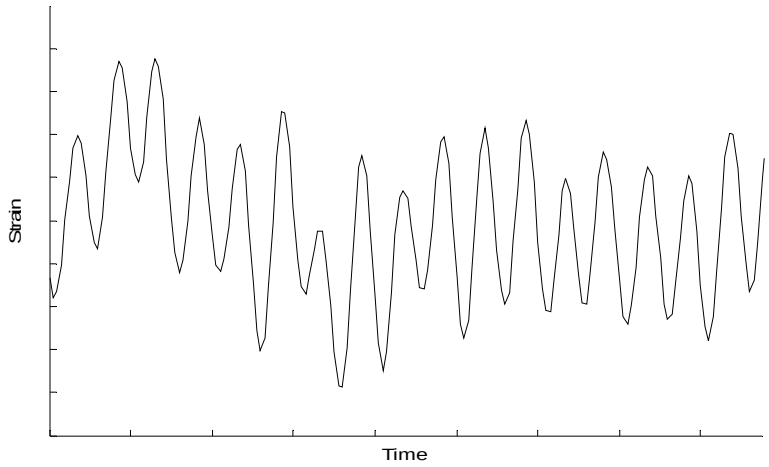

Figure 4.1 – Complex Load History

An important fact when performing cycle counting on variable amplitude loading histories must be noted. Due to the nonlinear relationship between stress and strain (plastic material behavior) the order in which cycles are applied can have a huge impact on the calculated fatigue life. Blocks of cycles can be grouped in many different ways i.e. 'low-high' (small amplitude cycles applied before larger amplitude cycles), 'high-low' (large amplitude cycles applied before smaller amplitude cycles), random, etc. and thus, are dependent on the order in which cycle amplitudes are applied. Much research has been conducted in order to understand the effect of block sequencing on fatigue life. It has been found that a 'low-high' sequence results in a fatigue life similar to or shorter than (thus conservative) the test life achieved using the original signal. A 'high-low' sequence results in a fatigue life much greater than the test life achieved using the original signal and is thus non-conservative. Other block sequencing arrangements yield intermediate fatigue lives [4, 24].

4.2 Cumulative Damage

As defined earlier, an engineering component's total life can be separated into crack initiation and propagation stages. Thus, there are different approaches used in determining cumulative fatigue damage in regards to the safe-life and damage-tolerant approaches for fatigue.

4.3 Miner's Rule

The linear cumulative damage hypothesis was first proposed by Palmgren[36] as early as 1924 and further developed by Miner[37] in 1945. This empirical damage summing method for the initiation phase as determined by either the stress or strain life approach is best known as Miner's Rule.

The load history as shown in Figure 4.2 consists of two blocks of constant amplitude loading, making up a variable amplitude load history. If the loading consists of only the largest cycle, S_{a1}, and it is assumed this load history will be repeated until failure, the engineering component will be exposed to a constant amplitude load history. Failure as defined by Miner's Rule occurs when:

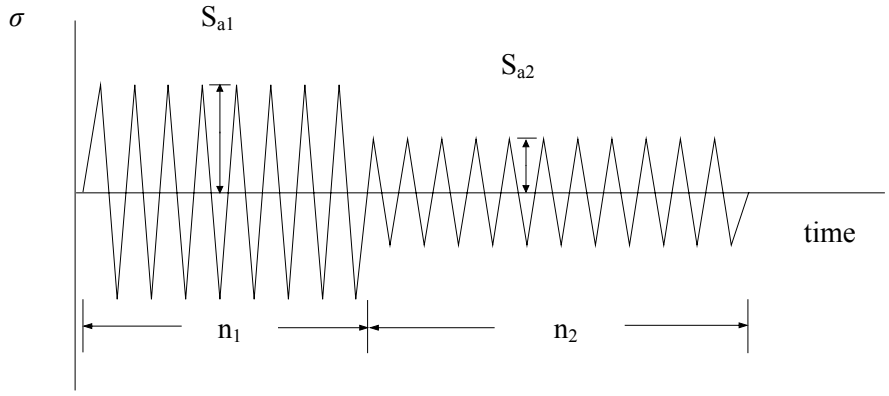

Figure 4.2 – Palmgren-Miner Rule for Life Prediction of a Variable Amplitude Loading

$$\frac{n_1}{N_1} = 1 \tag{35}$$

Where:

n_1 = the number of cycles at stress level S_{a1}

N_1 = the number of cycles to failure as obtained from the fatigue life endurance curve

The failure criterion for variable amplitude loading is simply the summation of the life fractions for each loading block, thus damage (B_f) is defined as

$$B_f = \frac{n_1}{N_1} + \frac{n_2}{N_2} + \frac{n_3}{N_3} + \ldots = \sum_{i=1}^{m} \frac{n_i}{N_i} = 1 \tag{36}$$

An alternative form of Miner's rule has been proposed by Madayag[38].

$$\sum_{i=1}^{m} \frac{n_i}{N_i} \geq X \tag{37}$$

Where:

X = the desired factor of safety and is selected on the basis's of the load history, usually less than 1

According to Reference [2], 90% of all naval aircraft are expected to obtain a service life without cracking. Therefore factors of uncertainty are used to provide a degree of assurance against premature service lives. A factor of 2 which is the ratio of the failure life to the desired life is often used. This in turn results in the variable X of Equation (37) to have a value of 0.5. Thus the fatigue life expended (FLE) is the cumulative damage with the factor of safety applied.

5 STANDARIZED LOAD SPECTRUM

One of the more significant inputs in determining service life is the load spectrum [2]. The loading spectrum chosen for the validation portion of this work was that of a generalized helicopter loading sequence developed in a collaborative study by three European countries, which resulted in the development of two standardized spectra. The first is referred to as Helix and it is a loading sequence representative of hinged articulated rotors. The second spectrum, called Felix, is a loading sequence representative of fixed or semi-rigid rotors [39]. The load spectrum, Felix/28, is a shortened version of the Felix spectrum and consists of 161,034 cycles through one pass, while the full Felix sequence has over two million loading cycles through one pass.

The Felix spectrum is scaled in Felix units with a maximum load in the sequence being 100 units. The ground load at landing is -28 Felix units and all alternating loads below 16 Felix units were omitted. The Felix/28 spectrum was developed further by omitting all alternating loads below 28 Felix units.

One pass through the spectrum represents a total of 140 flights, which can be divided into four flights at three different durations. The three different durations are 0.75, 2.25, and 3.75 hours which combines to represent 190.5 flight hours. The four types of flights represent loading sequences for either Training, Transport, Anti-Submarine Warfare (ASW), or Search And Rescue (SAR). Figure 5.1 shows a typical loading sequence for the Transport mission of the Felix/28 loading sequence.

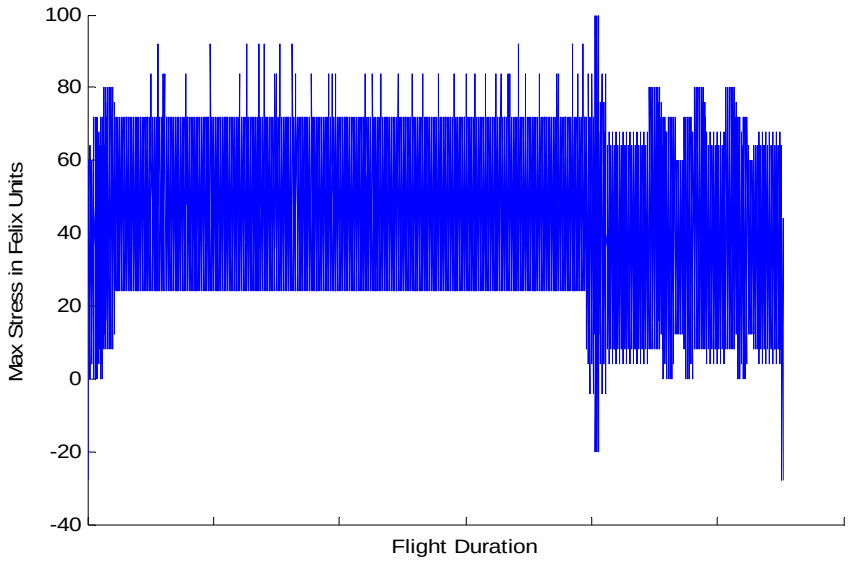

Figure 5.1 – Felix/28 Long Transport Flight (3.75 hrs)

6 MULTIAXIAL FATIGUE

6.1 Introduction

The fatigue theories introduced thus far can only be applied under the conditions of uniaxial stress states. In many applications, engineering components experience biaxial states of stress as a result of combined loading due to bending and torsion. In this thesis, the discipline of multiaxial fatigue will only be introduced as it continues to be a topic of concentrated research. However, a general field of knowledge on multiaxial fatigue analysis methods is emerging [4].

Bannantine and Socie [40] conducted research on the effects of multiaxial fatigue on the test specimen shown in Figure 6.1. The test specimen was tested under a typical service loading history with experimental results giving a test life of 600 repeats. However, when a uniaxial strain fatigue analysis at the fillet radius was used, a non-conservative life of 5000 repeats was calculated. They concluded that the factor of 8 in life estimation was because biaxial stresses were produced in the fillet radius. As discussed previously, transverse strains along the width of the notch cannot develop due to the constraint imposed by the lower (elastically) stressed material surrounding the plastic zone. This constraint does however produce a transverse stress. This study was a good demonstration of how a simple uniaxial loading can produce a biaxial state of stress at the notch.

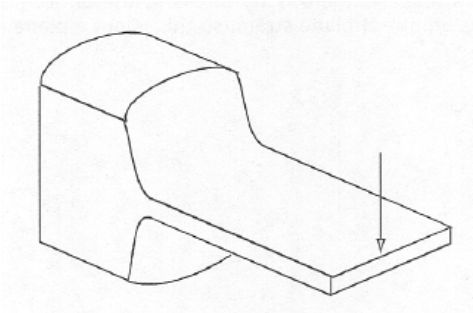

Figure 6.1 – Test Specimen for Multiaxial Fatigue

6.2 Strain-Based Models

The three essential features of the strain-life methodology for fatigue consists of the stress-strain relationships, the stain-life relationship, and Neuber's rule which is used as an elastic to elastic-plastic correction factor. Therefore, each of these must be extended in order to handle biaxial stress states in low cycle fatigue in which plasticity may occur.

If nodal stresses are biaxial and the direction of the principal stresses do not change during the load history, Neuber's uniaxial elastic-plastic correction factor can be extended to the following relationship.

$$\Delta\sigma_{ij} + \Delta\varepsilon_{ij} = \Delta\sigma_{ij}^{e}\Delta\varepsilon_{ij}^{e} \tag{38}$$

However, the complexity of this equation increases for cases where the principal stresses change direction.

Findely developed a theory for which it was proposed that fatigue damage under multiaxial conditions is a combination of both shear and normal stresses. An example of this is shown in Figure 6.2. With only a shear strain applied to the crack face, the shear load experienced by the crack tip is reduced due to the friction of the mating faces. However, with the addition of the applied stress normal to the plane of the crack, the crack faces will

separate. The application of the normal stress will cause the crack tip to experience the entire applied shear load by eliminating the friction between the mating faces [41].

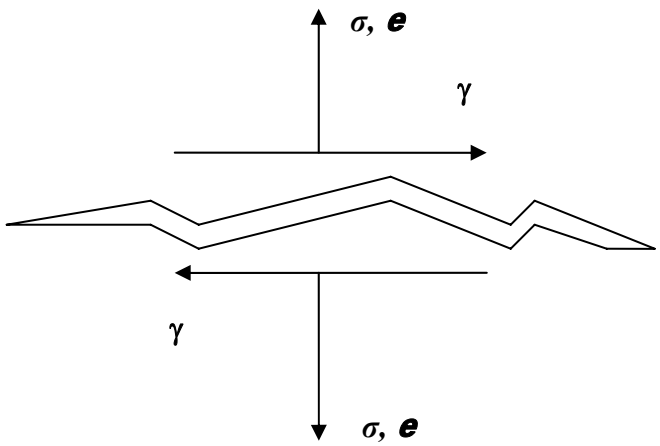

Figure 6.2 – Shear and Tensile Load Applied at Crack Faces

Currently, one of the more widely used models for predicting crack initiation of ductile metals due to multiaxial loading is the Brown-Miller criterion. Brown and Miller extended Findley's theory to incorporate strains. They proposed that the maximum fatigue damage occurs on the plane which experiences the maximum shear strain amplitude. The complete criterion is given by the following relationship [42]:

$$\frac{\Delta\gamma_{\max}}{2}+\frac{\Delta\varepsilon_N}{2}=1.65\frac{\sigma_f^{'}}{E}\left(2N_f\right)^b+1.75\varepsilon_f^{'}\left(2N_f\right)^c \tag{39}$$

Where:

γ_{max} = the maximum shear strain

ε_N = the strain normal to the plane which experiences the maximum shear strain amplitude

As discussed in Section 3.3.5, mean stress effects can have a significant impact on fatigue life. Thus, Morrow's mean stress correction can be included in the Brown-Miller relationship. The constants 1.65 and 1.75 are derived based on the assumption that the Poisson ratios for elastic and plastic stresses are 0.3 and 0.5, respectively, and that cracks initiate on the plane of maximum shear strain. However, the values of these constants will change under complex variable amplitude loading due to the effects of the varying damaged plane, but the values shown here are almost universally accepted [4].

Other methods, such as the principal strain criterion is often used for the analysis of brittle metals. By replacing the axial strain in Equation (21) with the principal strain, a multiaxial fatigue criterion which only requires uniaxial materials data can be developed.

6.3 Critical Plane

Principal strains can change their orientation during multiaxial load histories, necessitating the use of a critical plane analysis. In these cases it is not always obvious which plane will experience the most severe strains because the phase relationship between stresses is not always constant when components are subjected to multiaxial loading. Critical plane methods resolve the strains onto a number of planes and calculate the damage on each plane. Therefore a successful model should be able to predict both the fatigue life and the dominant failure plane(s) [41]. Additionally, because of the different possible failure modes, no single damage model should be expected to be used universally.

From the initial work of Brown and Miller, several modifications and additions have been formulated for the development of new critical plane multiaxial fatigue theories. These include the Socie-Bannantine criterion [40], the Fatemi-Socie criterion [43], the Wang-

Brown criterion [44], the Brown-Miller (developed with Kandil) criterion [42], and the more recent proposal by Chu, Conle and Bonnen [45].

There is currently a large amount of research in the area of life prediction due to multiaxial fatigue. McDiarmid[46] developed a multiaxial fatigue criterion that requires additional materials data but can be used for high cycle fatigue. For a comprehensive treatment on multiaxial fatigue it is suggested that the reader review reference [41]. However, Draper[4] recommends three criteria in performing fatigue analysis under multiaxial loading. The Brown-Miller criterion with mean stress correction is recommended for ductile metals, the Principal (or axial) strain criterion with mean stress correction is recommended for brittle metals and the Dang Van criterion [47] is recommended for infinite life design. These recommendations are based strictly on experience and experimental testing.

7 FATIGUE ANALYSIS FROM FINITE ELEMENT METHODS

Finite element analysis (FEA), also called the finite element method (FEM), is a method of analyzing engineering components in which the geometry of the structure is discretized into a series of nodes and elements. Using this numerical technique, a solution in terms of stresses, strains, deflections, temperatures, and frequency response can be obtained. These results, in turn, can be used for fatigue analysis. Fatigue analysis software uses stress results from a linear elastic FE analysis.

Fatigue analysis from FEA models is a fairly new subject, and many of the analysis rules have yet to be established. However, since crack initiation predominately occurs on the surface of a component, nodal stresses are generally the preferred approach over integration point stresses and averaged elemental stresses [4, 6]. Additionally, life prediction is dependent on the accuracy of both the stress analysis and the fatigue damage analysis. Chu[19,20] has stated that a 10% error in the stress calculation is likely to double the error in the calculation of fatigue damage. Therefore, careful attention must be given to geometry details, mesh density, load history, and material properties.

In a typical FE analysis, elements are joined at nodes, with each node having several values of stress calculated from adjacent elements. FE codes generally average these stresses, resulting in a single average nodal stress tensor for each node in the model. A good indication of the quality of the mesh is the difference between the averaged and un-averaged stresses at a node.

From linear elastic FE analysis, the elastic stresses are converted to elastic-plastic stress/strain using Neuber's rule or the Seeger-Hueler method. The Seeger-Hueler method is

used primarily in the special case in which the nominal stress approaches the yield stress, in which an elastic-plastic FEA could be used [4].

To ensure that Miner's Rule gives adequate life estimates for most engineering applications, fatigue analysis codes reduce the stress or strain amplitude at the endurance limit, which is determined from a constant amplitude test by 20% to 25%. This has become a common practice since under variable amplitude loading the endurance limit may disappear or its amplitude may be reduced [48].

Analyzing a linear elastic model with a single applied load history will consist of a finite element load case solution for the stresses at each node. The elastically calculated stress tensor for each node is multiplied by the load history to give a time history of the stress tensor. Fatigue software is used to calculate the time histories of the in-plane principal stresses and their corresponding directions at the surface of the model. The strain time history is then used in a strain life fatigue calculation and the process is repeated for each node in the model [4, 6].

As previously discussed, many components such as a car suspension system may have loads applied at several different points, resulting in multiple load histories. The FE analysis is used to calculate the stresses for each load case separately. Many fatigue analysis software codes are capable of analyzing components with multiple load histories applied to the model. In the fatigue analysis software, each stress data set is multiplied by the corresponding load history and the stress results are superimposed. The fatigue life is then calculated using a multiaxial Neuber's rule. If the principal stresses and strains are not constant (i.e. the load histories are not in phase) a critical plane analysis should be carried out

to determine the most damaged plane at each node. Thus, the location of the most damaged node can be determined and it does not necessarily have to be located at the node of maximum stress.

Major advances have been made in fatigue analysis software over the past decade and the correlation between predicted fatigue life and fatigue life based on test results are improving. Software such as fe-safe and FE-Fatigue are able to predict hotspots and actual fatigue lives with relative accuracy and reasonable processing speed. This is accomplished using either the stress-life method or the strain-life method. Once the hotspots are determined the results can be exported back into a FEA code to determine crack propagation and fracture if necessary. The flow chart in Figure 7.1 outlines a FEA-based durability analysis procedure.

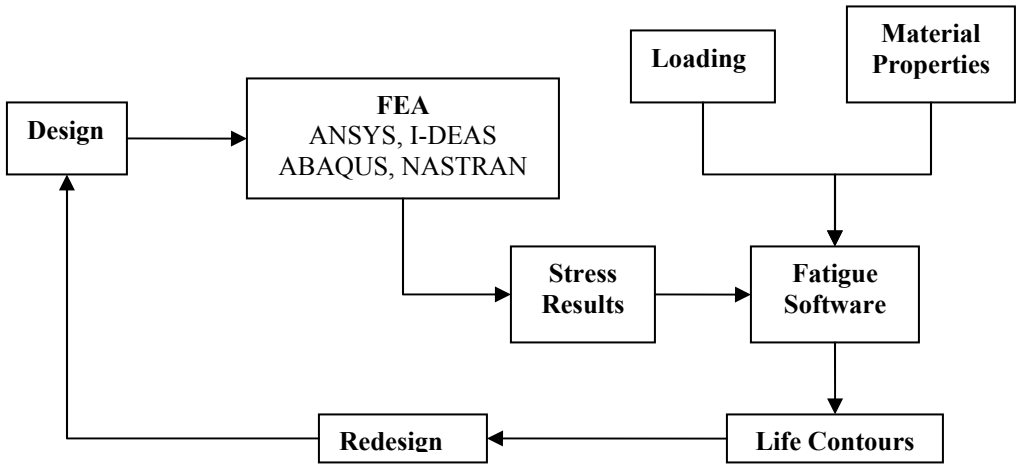

Figure 7.1 – Finite Element-Based Durability Analysis [6]

8 COMPUTER SOFTWARE DESCRTIPTION AND VALIDATIONS

8.1 Fatigue Modeling Software Description

For this work, the commercially available software suite fe-safeWorks developed by Safe Technology Limited was used. Safe Technology is recognized as a world-wide leading supplier of durability software and consulting services. In particular, Safe Technology is the leader in multiaxial fatigue analysis solutions. Safe Technology was formed in 1987 as John Draper & Associates. The software suite has been used to optimize the design of an automotive suspension component for durability under multiaxial loading.

The fe-safeWorks suite was chosen for several reasons. The fe-safeWorks suite encompasses three main software products: fe-safe Professional, fe-safe4fatiuge, and fe-safe LE. The software can be expanded by including numerous optional add-on modules, including the recent development of the Verity structural stress method. Battelle has licensed the revolutionary mesh insensitive method, which allows for the prediction of failure locations and calculated fatigue lives of welded joints of structures, to Safe Technology. Additionally, fe-safe is well-suited for analyzing all aspects of life-prediction of both 2-D and 3-D components under uniaxial or multiaxial loading. The primary focus of this research is on life-prediction of a single simulated component, but future work could address the entire structure in question and incorporate the software's signal-processing package for measured or simulated signals. The fe-safe software also offers the flexibility to interface with multiple finite element analysis software codes

8.2 ANSYS Overview

Preprocessing is the first step for a fatigue analysis. The steps consist of creating the model and mesh and specifying the material properties, loads, and boundary conditions. Fe-safe can read FEA data (stresses, strains, and temperatures) from several other third-party software files. ANSYS [49] was chosen for its geometry modeling and high quality meshing capabilities along with the additional benefit that fatigue results can be post-processed directly in ANSYS.

8.3 FE-SAFE Overview

The selection of an appropriate fatigue analysis solver is an important step in developing and analyzing the life-prediction of a part. Fe-safe was selected as the durability solver for fatigue life-prediction of metallic components. The commercially available software package calculates the fatigue lives at each node using a cycle-by-cycle analysis. Fe-safe provides comprehensive life-prediction capabilities for a wide range of two- and three-dimensional geometries. Capabilities include calculating where a 0.03 inch fatigue crack will occur, when a fatigue crack will initiate, factors of safety on working stresses, the probability of survival at different service lives, and a comprehensive materials database with a user-defined option. In addition, fatigue analysis can be performed from measured signals of three-element strain gage rosettes. Either stress life or strain life analyses can be performed with the use of uniaxial or multiaxial fatigue algorithms.

9 CLASSICAL MODEL VALIDATION ANALYSES AND RESULTS

9.1 Classical Model – Constant Amplitude Loading

In order to gain an understanding of fatigue methodologies and their use, a classical model consisting of an isotropic flat plate with a centrally located hole was analyzed under constant amplitude loading. Following previous studies published by Everett[7,8], the identical geometry and material properties of the test specimen were used. This classical model was used to validate the results obtained from a fatigue analysis using the commercially available software code fe-safe by comparing with the experimental results obtained by Everett. The geometry of the flat plate is shown in Figure 9.1.

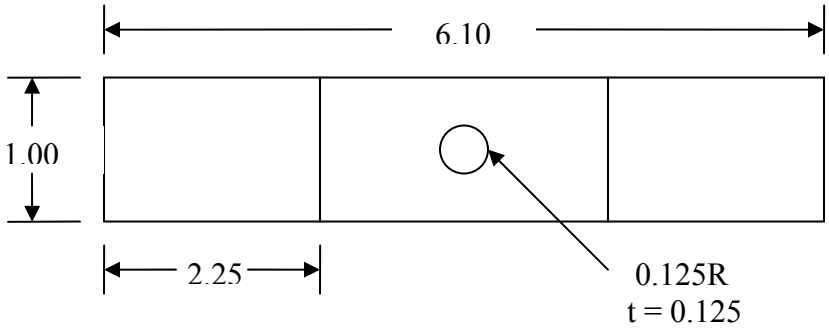

Figure 9.1 – Fatigue Test Specimen Configuration (dimensions in inches)

As discussed in Section 3.3, several material properties are needed for a strain-life fatigue analysis. Constant amplitude tests were conducted by Everett to produce the stress life curve as shown in Figure 9.2. Maximum net-section stress values ranged from 50 to 175 ksi with all tests having a stress ratio, R, equal to zero. Additionally, the net-section stress concentration factor for the plate geometry was 2.42. Using the data derived by Everett, the local strain curve fit material parameters are given in Table 9.1.

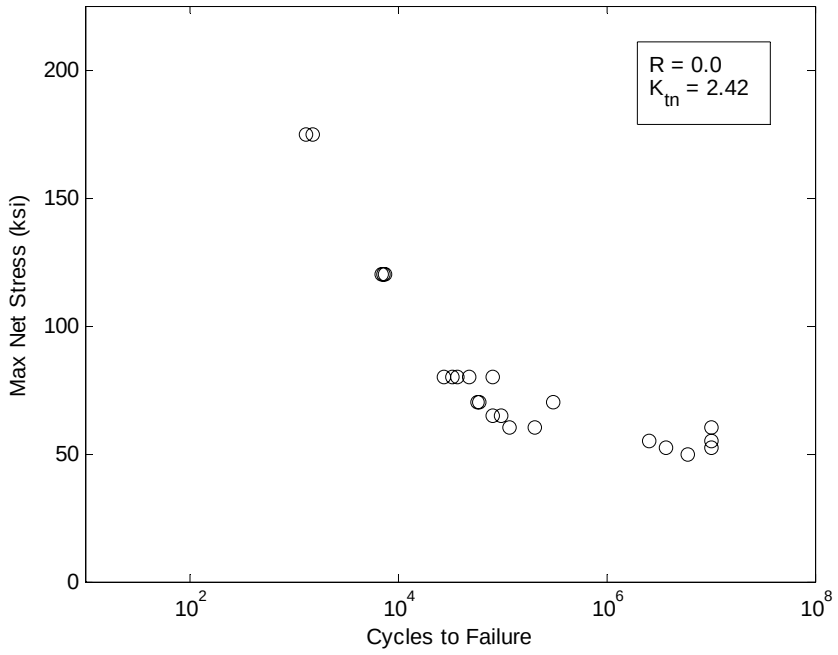

Figure 9.2 – Constant Amplitude Test Data [7, 8]

Table 9.1 – Material Properties for AISI 4340

σ_u	ultimate tensile strength	212 ksi (1)
σ_e	endurance limit	55.83 ksi (1)
σ_f'	fatigue strength coefficient	290 ksi (1)
b	fatigue strength exponent	-0.091 (1)
ε_f'	fatigue ductility coefficient	0.48 (1)
c	fatigue ductility exponent	-0.60 (1)
K	strain hardening coefficient	305 ksi (1)
n	strain hardening exponent	0.15 (1)
E	Modulus of Elasticity	30,000 ksi (2)
ν	Poisson's Ratio	0.3 (2)

Notes:
(1) – Values from the work of Everett [7, 8]
(2) – Values taken as typical aircraft quality [50]

A finite element analysis of the flat plate was conducted using ANSYS. Because horizontal and vertical axes through the center hole are axes of symmetry, only one quadrant

of the plate was analyzed. The applied loading was that of a unit cross-section load equivalent to a nominal stress of 1.0 ksi. The application of a unit load was used for ease of conducting a fatigue sensitivity analysis in fe-safe and since the ANSYS FEA code uses the stress concentration factor for which the reference stress is based on the gross-sectional area. For the geometry shown in Figure 9.1, the gross-section stress concentration factor was calculated to be 3.24. The choice of element type depends solely on the application. For the simple 2D isotropic flat plate geometry subjected to a uniform uniaxial far-field stress the most appropriate element was the quadrilateral. The 4-node quadrilateral element has compatible displacement shapes and is well-suited for modeling curved boundaries. The model was analyzed as plane-stress with a thickness condition.

The results computed by a finite element analysis may not agree with the exact solution due to a variety of sources for numerical errors. Discretization errors are influenced by the element type, element size and shape, and the imposed boundary conditions and constraints. For a classical problem, such as a flat plate in plane stress, the convergence rate provides a good indication of the accuracy of the numerical model. Mesh refinement was performed until the numerical results at the location of the stress concentration converged with the exact solution as obtained from reference [32]. Figure 9.3 shows the sufficiently refined mesh generated by ANSYS. The nodal stress solution of the flat plate with a unit applied load is shown in Figure 9.4. As expected the maximum normal stress is 3.247 ksi, which is located at node 3 of element 599.

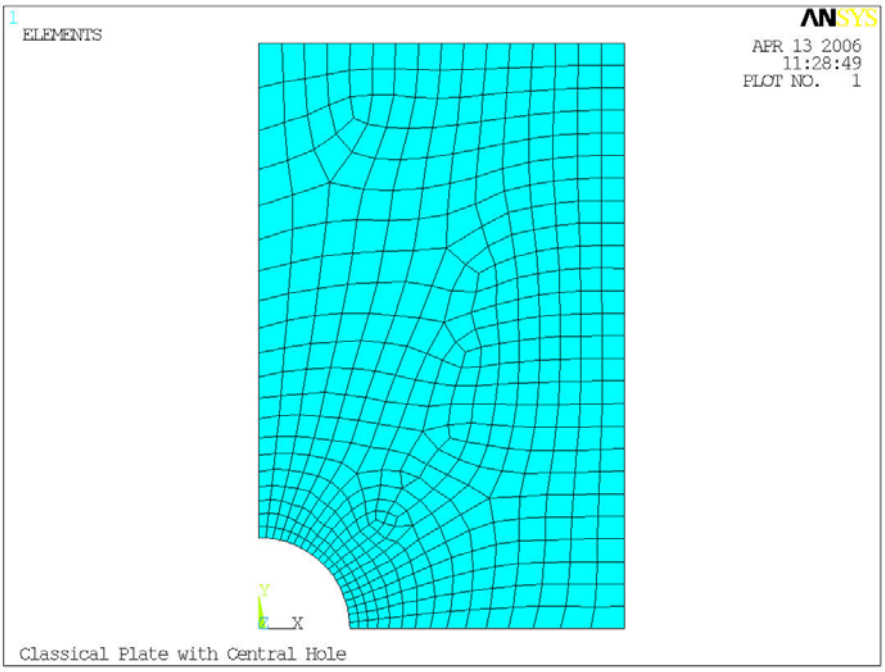

Figure 9.3 – Quadrilateral Meshing Scheme

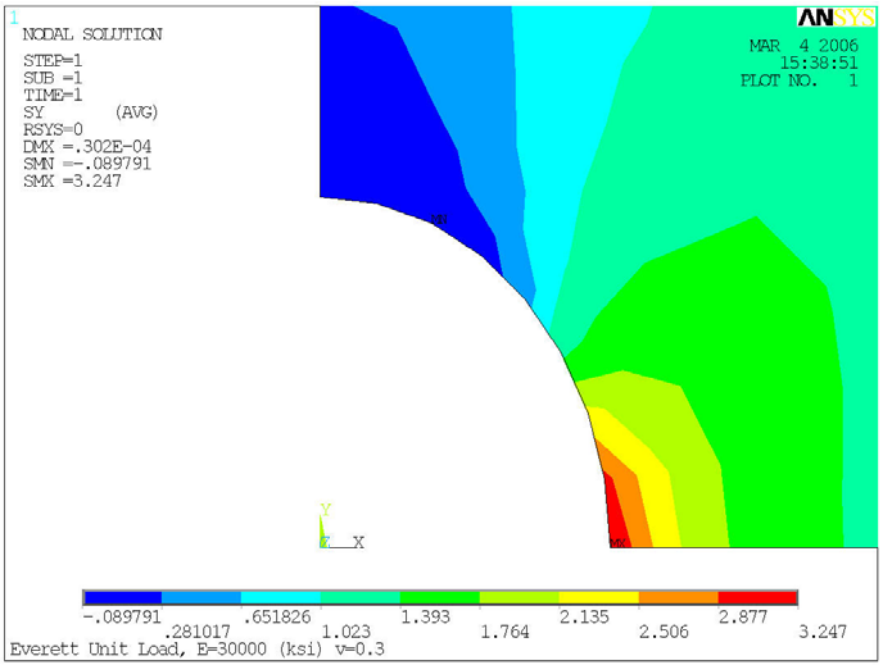

Figure 9.4 – ANSYS Stress Results for a Unit Applied Load (ksi).

To perform a fatigue analysis, ANSYS RST files (*.rst) are imported into fe-safe. The appropriate material is then selected. Although fe-safe is supplied with a comprehensive database containing fatigue properties for commonly used materials, a new material was created based on the material properties from Table 9.1 and Figure 9.2. This is accomplished by creating a new database based on a template from the user's directory within fe-safe. Accurate materials data is essential for life prediction. Table 9.2 compares numerically simulated fatigue lives based on a Brown-Miller with Morrow mean stress correction for standard SAE 4340 steel and the 4340 steel used in reference [7, 8]. The percent difference between the calculated fatigue lives demonstrates the importance of accurate material properties for life prediction. The materials data text file is given in Appendix A.

Table 9.2 – Fatigue Life Comparison for Different 4340 Steels

	SAE 4340[27]	Everett 4340[7,8]		Applied Load	SAE 4340 Fatigue Life	Everett 4340 Fatigue Life	% Difference
σ_u	180	212		50	296135	1829360	144.27
σ_e	-------	55.83		52.5	197274	1127047	140.42
σ_f'	285	290		55	136095	721537	136.53
b	-0.102	-0.091		60	72140	331455	128.50
ε_f'	1.223	0.48		65	42007	170061	120.77
c	-0.734	-0.60		70	26533	95109	112.75
K	270	305		80	12403	37129	99.84
n	0.137	0.15		120	1897	3515	59.79
E	28000	30000		175	485	645	28.32
ν	0.33	0.3					

Next, a constant amplitude load with a mean stress (R = 1) was applied to the model. This was accomplished with the use of a load definition file (LDF) which was created in a text editor. The LDF file in its simplest form is defined as a series of blocks. Each loading

block can define a dataset sequence, a number of repeats of the block, and other parameters such as a scaling factor. The LDF filed used for a constant amplitude load which consists of one block and scaled accordingly is given in Appendix B.

As discussed in earlier sections, careful consideration must be given to the selection of the appropriate algorithm for fatigue analysis. Fe-safe provides the flexibility of selecting both stress or strain life methodologies and the choice of a fatigue algorithm based on either uniaxial or multiaxial loading. Several simulations were computed using the different fatigue algorithms and the results were compared with the experimental test results of Everett.

Figures 9.5 through 9.7 show fatigue life variations for different strain-life algorithms and the results are compared with constant amplitude test data. Figure 9.5 utilizes a uniaxial Principal Strain algorithm with mean stress correction based on both Smith-Watson-Topper and Morrow. It can be seen from this figure that both algorithms predict the fatigue life with reasonable accuracy when compared with the experimental data. A Morrow mean stress correction predicts the fatigue life with reasonable accuracy at low cycle fatigue. Good correlation between the SWT mean stress correction and the experimental data occurs as the cycles to failure are increased.

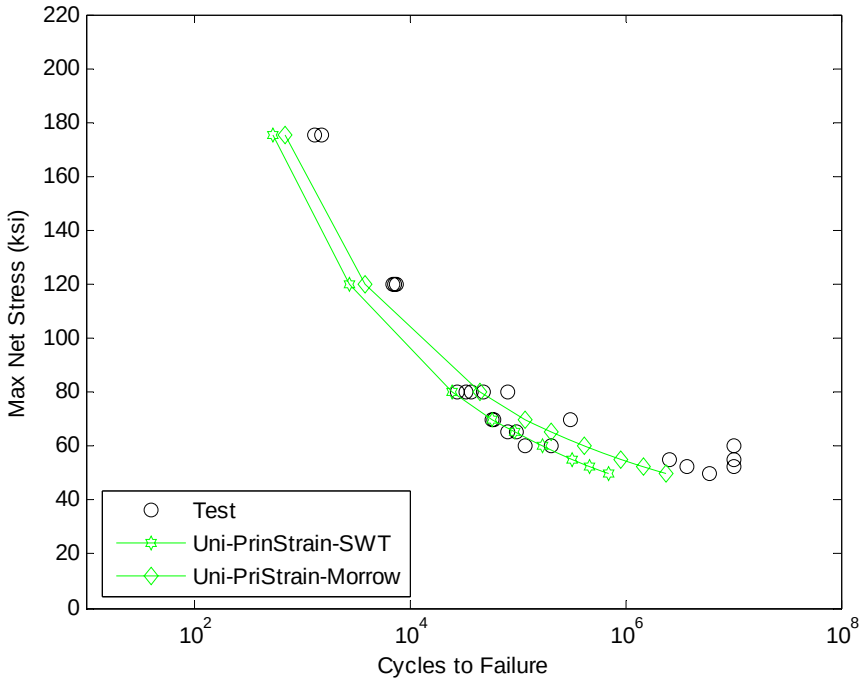

Figure 9.5 – Uniaxial Principal Strain Algorithms, Constant Amplitude Loading

Draper[4] recommends that a multiaxial Principal Strain approach be used for brittle metals. Figure 9.6 shows the life prediction utilizing this algorithm for the given material used in this research. It can be clearly seen that this approach predicts the fatigue life for low cycles to failure with the best accuracy. For mid-range to a high number of cycles, a higher life is predicted as compared with test results. This is particularly evident for life prediction using the multiaxial principal strain algorithm with no mean stress correction.

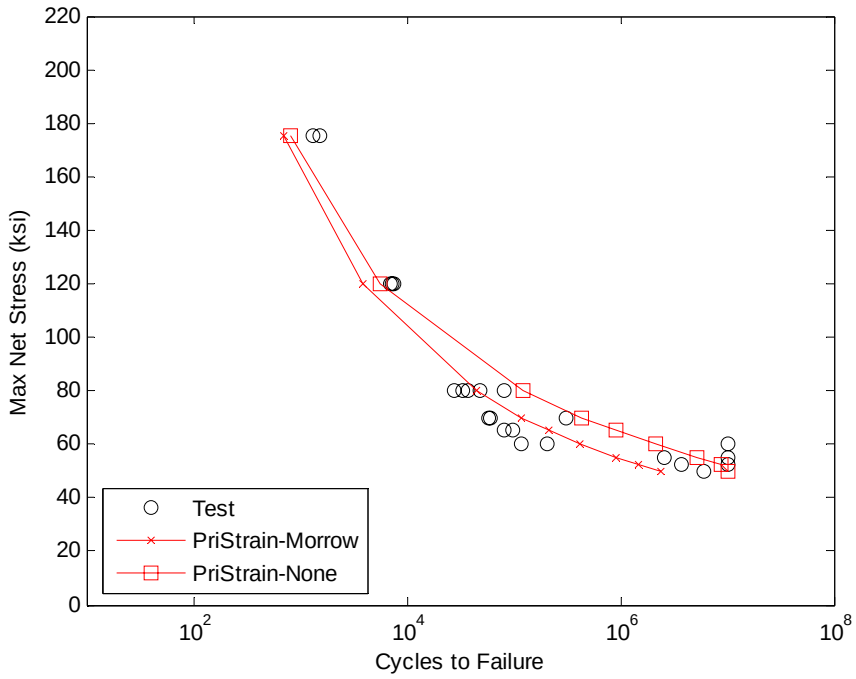

Figure 9.6 – Multiaxial Principal Strain Algorithms, Constant Amplitude Loading

Figure 9.7 utilizes a multiaxial Brown-Miller algorithm with both a Morrow mean stress correction and no mean stress correction. Both predict the fatigue life with reasonable accuracy. However, as the number of cycles to failure is increased the predicted fatigue life is greater than the test results, particularly in the case with no mean stress correction.

Figure 9.8 is a contour plot of the calculated fatigue life where the applied stress load equals 60 ksi. The contour plot is the result of a multiaxial Brown-Miller Morrow fatigue life calculated in fe-safe with the contour plot generated in ANSYS. The fatigue lives are represented in a $\log_{10}$ scale with the shortest life located at the stress concentration, as expected. For a value of 4.978, the calculated fatigue life is 95060 cycles. The fe-safe

output file for the constant amplitude loading of the analyzed flat plate using the multiaxial Brown-Miller strain life fatigue algorithm is given in Appendix C.

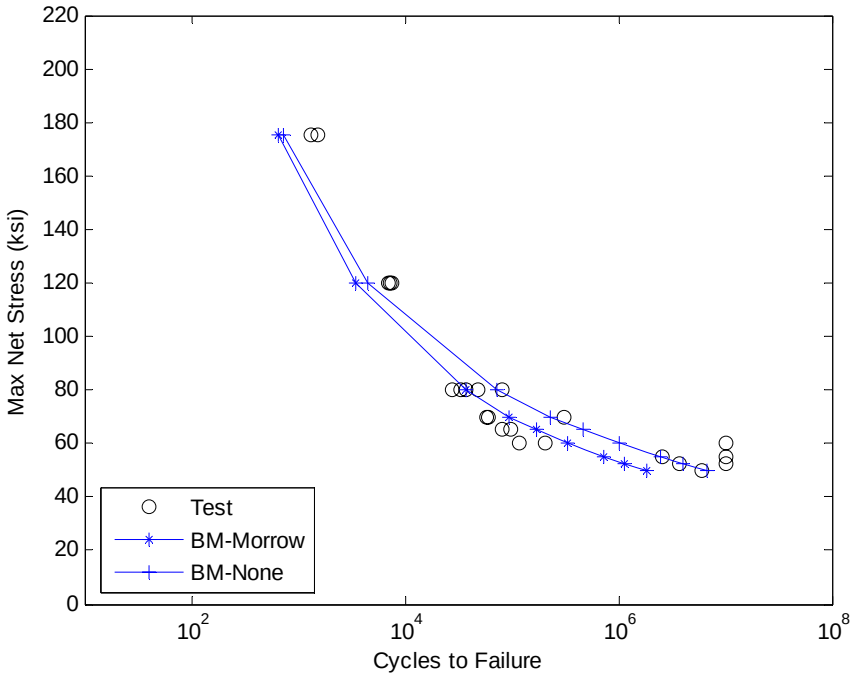

Figure 9.7 – Multiaxial Brown-Miller Algorithms, Constant Amplitude Loading

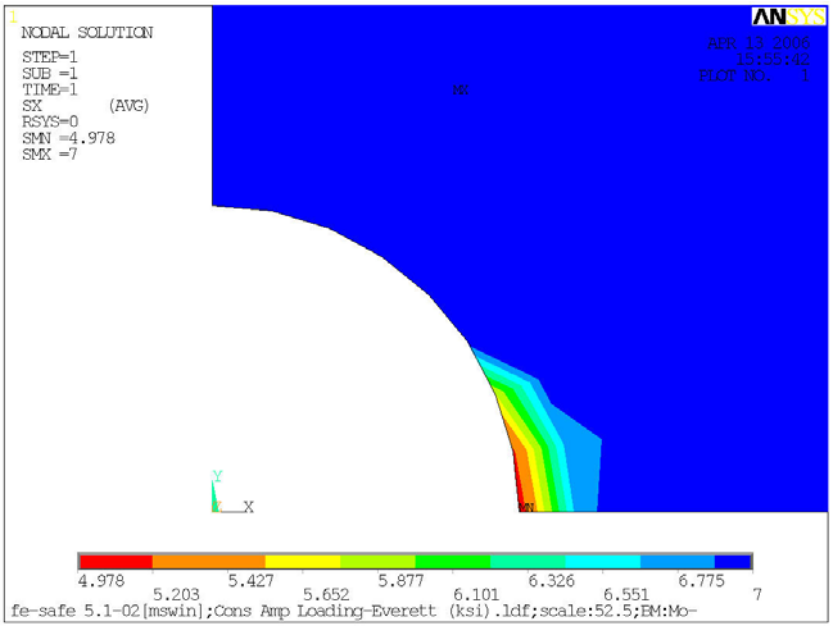

Figure 9.8 – Calculated Fatigue Life Damage Contours in Log_{10} Scale

Figure 9.9 shows the predicted fatigue life for two different uniaxial stress-life algorithms with Goodman and Gerber mean stress corrections. The stress life methodology does not account for the effects of plasticity and thus significantly under-predicts the fatigue life. Even in this simplest of test cases the stress life approach, while conservative, is not very accurate. An important fact must be noted. Within the fatigue community, calculated predicted fatigue lives within an order of 5 is presumed to be reasonable and a calculated life within an order of 2 is considered exceptional [51]. However, it is obvious that the use of this methodology would result in the replacement of useable aircraft components well before their designed fatigue life.

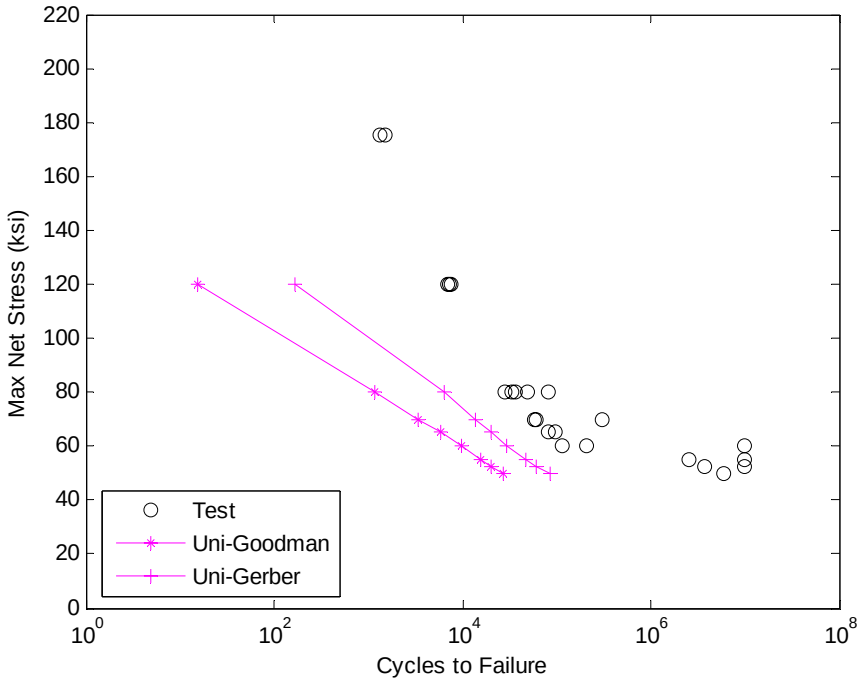

Figure 9.9 – Uniaxial Stress Life Algorithms, Constant Amplitude Loading

9.1.1 Classical Model – Conclusions

The elastic strain term of Equation (21) is dominant at long lives since the plastic strains are relatively small. This can be seen in Figure 3.8, which shows that as the number of cycles increases the strain curve approaches the elastic strain line, resulting in a narrow hysteresis loop. Conversely, for short lives the plastic strain term becomes dominant as compared with the elastic strains. This results in the strain life curve approaching the plastic strain line which is equivalent to an increase in the width of the hysteresis loop. Although a Brown-Miller with a Morrow mean stress correction is typically recommended for ductile materials, the results show that the best approach is dependent on the component geometry and loading. Under uniaxial loading a principal strain approach with a SWT mean stress

correction appears to be the best for intermediate fatigue lives. However, for both low and high cycle fatigue this approach gives the most conservative fatigue life. A multiaxial Brown-Miller with no mean stress correction predicts a fatigue life for a uniaxial constant amplitude loading at either low or high cycle fatigue with the greatest accuracy. Therefore, the engineer must have a good understanding of the different fatigue algorithms and their application to accurately predict the life of a component.

9.2 Classical Model – Variable Amplitude Loading

As discussed earlier, most components rarely experience constant amplitude loading under real-world conditions. Thus, the next step in validating the fatigue capability is to gain insight into the accuracy of numerically simulated life predictions under variable amplitude loading and to gain confidence in the results. Following previous studies published by Everett[7, 8], the model under constant amplitude loading was re-analyzed under a uniaxial variable amplitude load history. The loading, as described in Chapter 5, was a shortened version of the standardized Felix spectra, which represents a load sequence for fixed or semi-rigid helicopter rotors. The standardized loading spectrum was generated through the GENErator for SatandardIsed Sequences for fatigue (Genesis for Fatigue[52]) computer program. The Genesis for fatigue program is freely available upon request from the National Aerospace Laboratory NRL – The Netherlands. It was recommended by the developer of the Genesis program that the shortened version of the Felix spectra only be used when analyzing for long lives that are close to the fatigue limit. This is due to the method of omission of cycles [40]. Therefore, the normalized Felix/28 load spectrum, consisting of 161,034 cycles, was used.

The analysis for life prediction of the flat plate was similar to the analysis for constant amplitude loading in fe-safe with the exception of the applied loading. Again, a load definition file (LDF) was utilized to input the load history but one block now contained the text file containing the 161,034 cycles of variable amplitudes. The LDF file as well as the Felix/28 load spectrum is given in Appendix D.

Figure 9.10 shows the test results of the predicted fatigue lives for the Felix/28 spectrum which was run for several different maximum stress levels. Superimposed on this plot are the numerical simulation results from the Brown-Miller and Principal Strain fatigue algorithms. The different algorithms follow the trend of the Felix/28 test data fairly well, although the predicted fatigue lives are highly non-conservative. However, results from the Brown-Miller algorithm with a Morrow mean stress correction predicts the fatigue life particularly well at lower stress levels near the fatigue limit of the material.

As discussed in Section 4.1, fatigue analysis software performs a cycle counting technique for variable amplitude loadings. The complex loading is cycle-counted into a series of constant amplitude blocks, the order of which can be grouped in many different ways with each block loading sequence having a distinct effect on the fatigue life of the component. All variable amplitude loading spectra are blocked in a low-high grouping when analyzed in fe-safe. According to Reference [4], most other block loading patterns produce lives which are significantly longer than the lives obtained from the original service signals. This may explain the difference in predicted fatigue lives between the numerical simulations and test results. However, as was mentioned previously, the shortened version of the Felix spectra is typically recommended only for long lives near the fatigue limit. With this

understanding the Brown-Miller Morrow algorithm predicts the fatigue life with exceptional accuracy as the applied stress level approaches the endurance limit of 55.83 ksi.

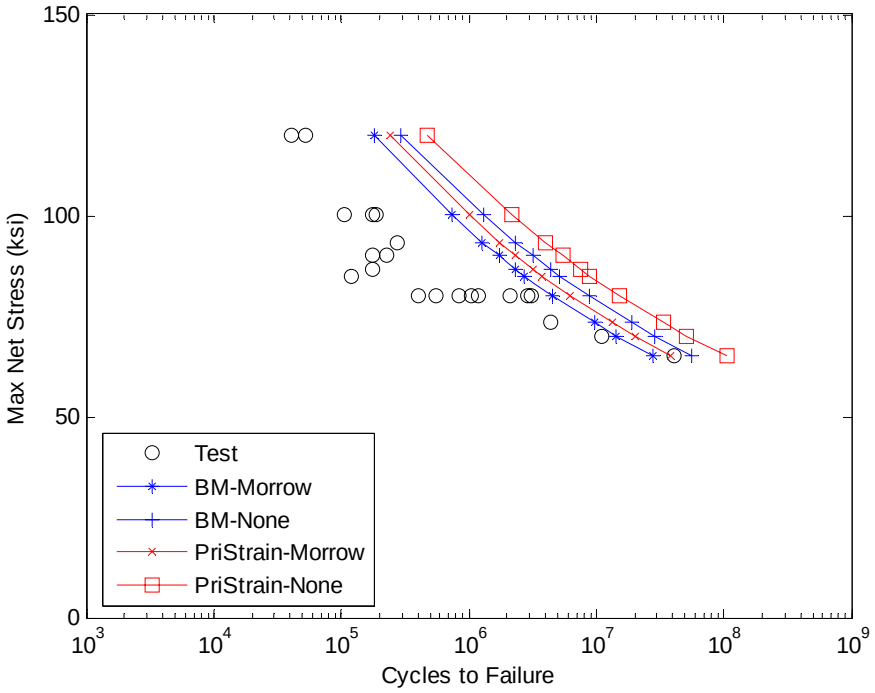

Figure 9.10 – Multiaxial Strain Life Algorithms, Felix/28 Spectra

10 MAIN LANDING GEAR DRAG BEAM ANALYSIS AND RESULTS

10.1 Background

Engineers are responsible for predicting the fatigue life of critical aircraft components for both military and commercial aircraft. Many of these aircraft are in service long beyond their design lifetime and due to the nature of quick response expeditionary requirements, they are subjected to extreme environmental conditions, such as desert sand and salt water environments. Thus, there is a need to predict the life of critical components for timely scheduling of maintenance.

Figure 10.1 – H-60 Naval Aircraft

As an example of a typical fatigue problem, consider the fatigue failure of the main gear drag beam as shown in Figures 10.1 and 10.2. Life prediction and maintenance scheduling of this component is critical as the consequences of premature failure can be catastrophic. The main gear drag beam is manufactured from ultra high strength 300M steel

(U_{ts} = 280 ksi). This steel also has a high fracture toughness and therefore widely used in helicopter landing gears. However, as with most ferrous alloys the material is vulnerable to corrosion fatigue and stress corrosion cracking. Corrosion fatigue by definition is the result of cyclic loading in a corrosive environment. It plays a major role in the degradation of cyclically loaded steel components that must operate in a seawater environment. Corrosion prevention often incorporates the use of a corrosion resistant material or applying paint, plating, etc. to the surface of the material. In addition to corrosion fatigue, stress-corrosion-cracking (SCC) may occur when a material is under a sustained static load or residual stress in a seawater environment. Hertzberg[53] provides an example of the degradation on the fracture toughness of AISI 4340. In an inert environment, AISI 4340 has a plane strain fracture toughness, K_{IC}, of 56 MPA $\sqrt{m}$, however, in seawater it has a K_{ISCC} as low as 17 MPA $\sqrt{m}$.

The drag beam can essentially be described as a step down tube where corrosion can occur inside the shaft. As noted earlier, Hoffman[2] describes the current maintenance procedure for corrosion as purely reactive in which corrosion is typically removed when it is detected. A cause of concern is that with the removal of corrosion within the shaft, the inner diameter is reduced and the design fatigue life might be reduced.

Corrosion is a common fleet issue and it is not aircraft specific. It has been estimated that nearly 4% of the US. Air Force annual budget is due to the effects of corrosion and it continues to increase each year [54]. Within the U.S. Navy it is estimated that 35-36% of all maintenance man hours over the last 10 years are due to corrosion problems. Additionally, it is estimated that 54-55% of all maintenance items processed over the last 10 years are

corrosion related [55]. One labor intensive corrosion prevention technique used within the U.S. Navy is frequent "washings" of all naval aircraft.

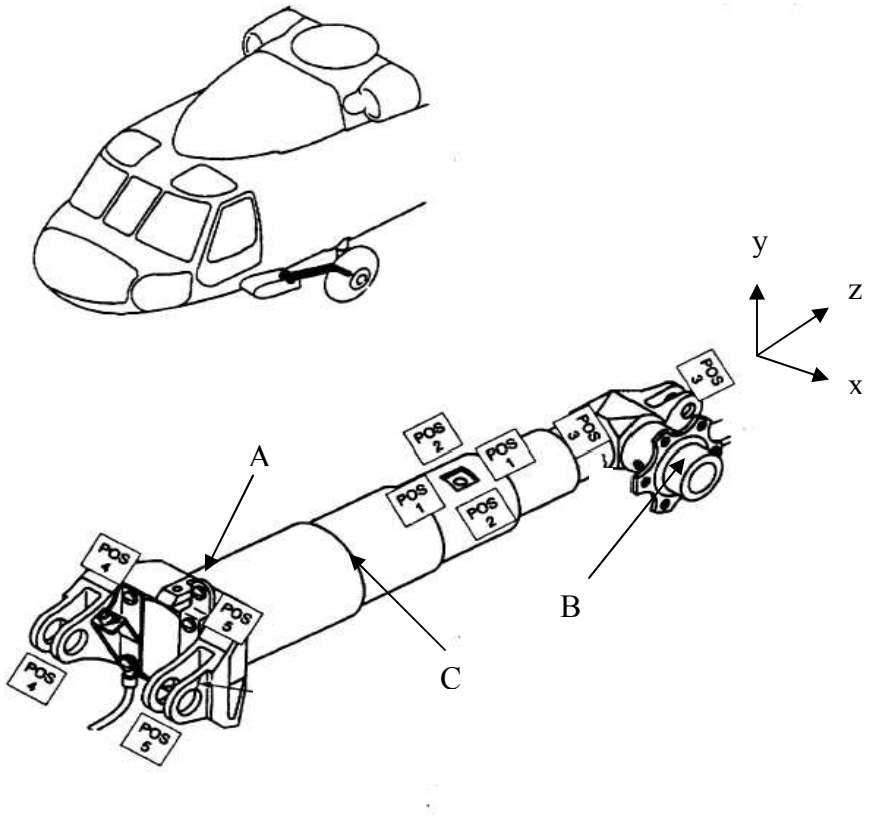

Figure 10.2 – Main Gear Landing Drag Beam [56]

As shown in Figure 10.2, the drag beam has a nearly fixed boundary condition at section A. Therefore, this section experiences high stresses. Complex loading consisting of axial, torsion, and bending are applied at section B. The current fatigue analysis procedure is to resolve the loadings into the drag beam axes and determine the stress state at location A. It was determined through a static analysis that section A undergoes a centric axial

compressive force of 1182 lbs, a twisting couple of 3636 in-lbs, and a resultant bending moment of 7300 in-lbs. A detailed derivation of the applied loading is given in Appendix E.

Consider first a stress-life approach for multiaxial fatigue. In this procedure, loadings are resolved into an effective stress amplitude and an effective mean stress. Utilizing stress invariants, the effective stress amplitude and the effective mean stress for any convenient coordinate axes can be determined from the following two equations,

$$\tilde{\sigma}_a = \frac{1}{\sqrt{2}}\sqrt{\left(\sigma_{xa}-\sigma_{ya}\right)^2+\left(\sigma_{ya}-\sigma_{za}\right)^2+\left(\sigma_{za}-\sigma_{xa}\right)^2+6\left(\tau_{xya}^2+\tau_{yza}^2+\tau_{zxa}^2\right)} \qquad (40)$$

$$\tilde{\sigma}_m = \sigma_{xm}+\sigma_{ym}+\sigma_{zm} \qquad (41)$$

Note that the various stress components are defined in the conventional manner with the addition of *a* and *m* indicating amplitude and mean, respectively.

As previously described in Section 3.2, S-N curves are commonly developed from bending or axial tests resulting in a uniaxial state of stress. Figure 10.3 is a typical S-N curve for 300M steel. Under a complex variable amplitude loading the stress-life approach requires the effective amplitude stress and the effective mean stress as determined from Equations (40) and (41) be combined into an equivalent completely-reversed uniaxial stress, σ_{ar}. The equivalent reversed stress amplitude is defined by the following equation,

$$\sigma_{ar} = \frac{\tilde{\sigma}_a}{1-\frac{\tilde{\sigma}_m}{\sigma_f^{'}}} \qquad (42)$$

Where $\sigma_f^{'}$ is the fatigue strength coefficient of the material. This procedure essentially reduces a complex state of stress into a uniaxial state of stress for determining fatigue life based on an S-N curve. The fatigue life based on the stress-life methodology is determined

by substituting σ_a of Equation (3) with σ_{ar} for each block in the load history. For the main gear drag beam a safety factor of 2 is applied to the equivalent reversed uniaxial stress as determined by the fillet radius. In addition to the applied safety factor due to the inherent stress concentration in the drag beam, other modifications are applied to the S-N curve. Because of various uncertainties in the actual service loads, statistical variations in the fatigue strength of the component, surface finish, and environmental effects, it is often difficult to quantify these variables. For this reason the S-N curve is often lowered in the stress direction or shifted in the life cycle direction, as shown in Figure 10.3. At this step in the stress-life approach, the Palmgren-Miner Rule (Equation 36) is applied to determine the total fatigue life due to a complex variable load history.

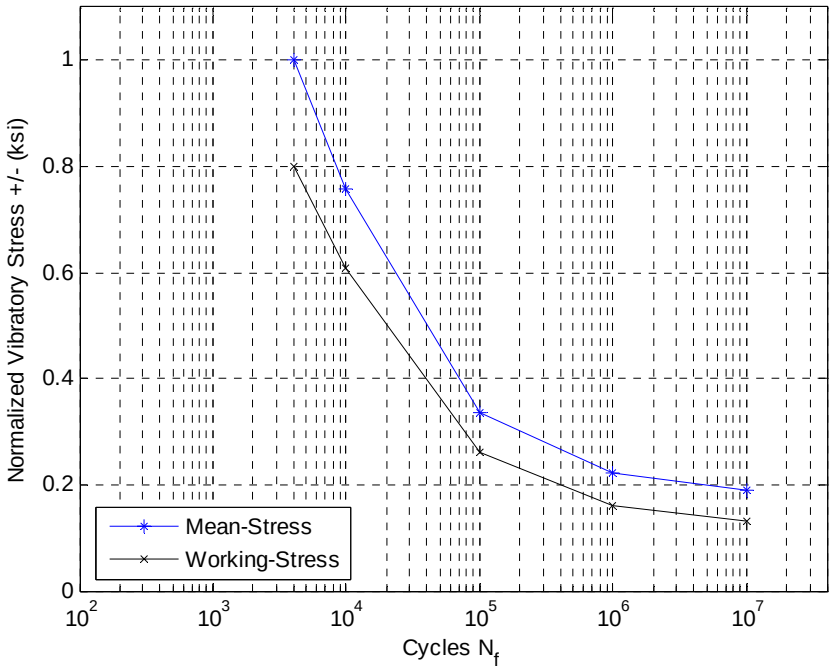

Figure 10.3 – S-N Curve for 300M Steel U_{ts} = 280 ksi

A typical load history for the drag beam along with the corresponding occurrence per 1000 flight hours is shown in Table 10.1. Utilizing the normalized S-N curve from Figure 10.3, the damage per 1000 flight hours for both the mean and working life can be calculated. Based on the stress-life methodology the calculated mean and working fatigue life at section A of the drag beam is 131,060 hours and 59,206 hours, respectively. A detailed analysis of the calculated fatigue life is given in Appendix E.

Table 10.1 – Life Calculations for Section A of the Drag Beam, 300M

Applied	stress at	Sect. A	Occur.	Mean		Working	
No.	Steady	Vibratory ±	1000 flt.	Cycles	Damage	Cycles	Damage
1	9155	9155	190	inf	0	inf	0
2	9783	9783	190	inf	0	inf	0
3	28320	28320	190	240000	0.00079	86000	0.00221
4	19980	19980	190	7000000	0.00003	360000	0.00053
5	12922	12922	150	inf	0	inf	0
6	15802	15802	150	inf	0	1300000	0.00012
7	43384	43384	150	54000	0.00278	27500	0.00545
8	30607	30607	150	170000	0.00088	69000	0.00217
9	17465	17465	35	inf	0	710000	0.00005
10	24415	24415	35	600000	0.00006	400000	0.00023
11	63870	63870	35	18700	0.00187	155000	0.00368
12	45061	45061	35	49000	0.00071	9500	0.00137
13	21866	21866	2.5	1700000	0	25500	0.00001
14	35248	35248	2.5	98000	0.00003	240000	0.00005
15	87972	87972	2.5	7000	0.00036	3200	0.00078
16	62065	62065	2.5	20400	0.00012	10500	0.00024
17	1894	3893	140	inf	0	inf	0
18	5511	10009	6	inf	0	inf	0
19	10504	19001	1	inf	0	460000	0
20	1894	4893	303	inf	0	inf	0
21	5511	12008	13	inf	0	inf	0
22	10504	20500	1	4400000	0	310000	0
23	1894	4893	23	inf	0	inf	0
24	5511	14507	1	inf	0	3000000	0
25	1894	5393	1	inf	0	inf	0
26	1894	5393	1	inf	0	inf	0
					Σ=0.00763		**Σ=0.01689**

10.2 Main Gear Drag Beam Model

In order to analyze the main gear drag beam with ANSYS and the fe-safe fatigue and durability code, a segment of the drag beam was modeled. As shown in Figure 10.4, a three dimensional view of the model was created in SolidWorks 2005 solids modeling software to better illustrate the section to be analyzed for fatigue. The three-dimensional view shows section AC with the addition of the attachment lug section (section AD) which is modified for applying the appropriate boundary conditions. Internal loads are calculated and applied to section C and the derivation of the applied loads is given in Appendix F. Table 10.2 shows the dimensions and applied load magnitudes for the drag beam.

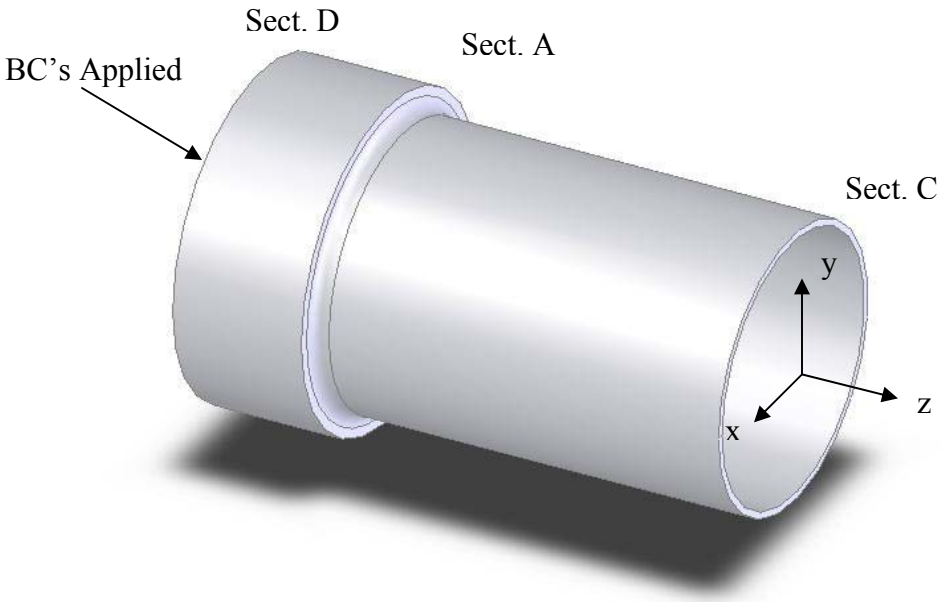

Figure 10.4 – Perspective View of Modeled Segment

Table 10.2 – Physical Dimensions Used in Simulations

Symbol	Definition	Value	Load Reactions at D	Value
BA	length of sect. BA	26.75 in	Fz	-1182 lbs
CA	length of sect. CA	6.75 in	T	3636 in-lbs
AD	length of sect. AD	3.25 in	Mx	7745 in-lbs
do	outer diameter of small tube	5.00 in	Ux	0
di	inner diameter of small tube	4.77 in	Uy	0
t	wall thickness	0.115 in	Uz	0
R_f	fillet radius	0.25 in	ROTx	0
Do	outer diameter of large tube	5.515 in	ROTy	0
Di	inner diameter of large tube	5.285 in	ROTz	0

10.3 ANSYS Analysis

The ANSYS finite element code was used to create a three dimensional finite element model of Figure 10.4, which represents the main gear drag beam. As with the classical plate analyzed previously, nodal stresses are needed as input to the fe-safe fatigue software code. Thus all three-dimensional finite element models created in ANSYS were solved using linear/static analysis. The material model used for the drag beam analysis was linear-elastic and taken to be equivalent to ASTM-A579-G72 steel. This steel grade correlates fairly well with 300M steel alloy. This steel grade is available in the materials database of fe-safe and its material properties, shown in Table 10.3, were therefore used for both the finite element and fatigue analyses.

Table 10.3 – ASTM-A579-G72 Material Properties [27]

σ_u	270.05 ksi	ε_f'	0.68	n	0.049
σ_f'	436.55 ksi	c	-0.752	E	27,000 ksi
b	-0.101	K	280.78 ksi	ν	0.33

The drag beam was modeled using four-node structural shell elements (SHELL43) in ANSYS. The SHELL43 element has six degrees of freedom at each node enabling translations in the nodal x, y, and z directions and rotations about the nodal x, y, and z axes [49].

The drag beam was created using keypoints to outline the basic geometry. The keypoints were placed at the mid-surface of the modeled thick-walled cylinder representing the presumed critical section of the drag beam. The keypoints were used to create lines and areas with the lines segmented for mesh refinement. Figure 10.5 contains perspective views of the drag beam model meshed with SHELL43 elements. The ANSYS batch file for this analysis is given in Appendix G.

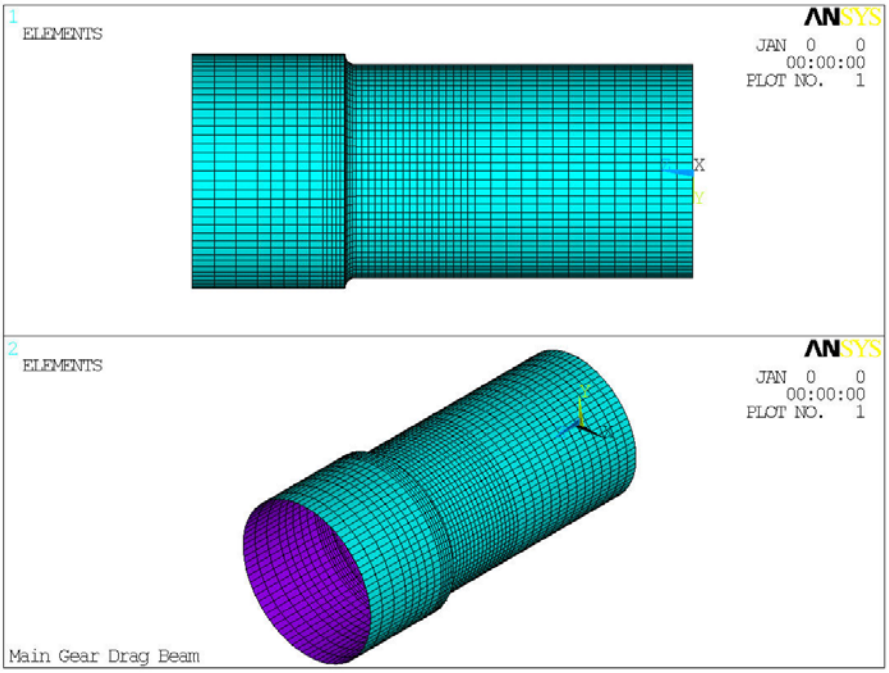

Figure 10.5 – Perspective Views of the Meshed Modeled Drag Beam Section

10.4 Boundary Conditions

Geometric boundary conditions and loads were applied to sections D and C of the drag beam FE model, respectively. Nodal displacements located at section D were set to zero, which represents a "wall" type boundary condition. The "wall" boundary condition involved constraining translational displacements in the global X, Y, and Z directions and constraining rotations about the global X, Y, and Z axes. The prescribed boundary force, moment, and torque loads shown Table 10.2 were applied to the nodes at section C.

To ensure the applied boundary conditions were applied far enough from the presumed critical area, a sensitivity analysis was conducted. The keypoints at section D were incrementally increased in the z-direction until nodal stress values at the critical location converged.

10.5 Illustrative Example

The goal of this research is to establish a procedure to analyze and predict the service life of a complex aircraft component and determine if a reworked part is suitable for continued service. As an illustration of this procedure, a benchmark simulation of a pristine drag beam component was developed for comparison with other simulations. The component shown in Figure 10.5 consisted of a uniform thickness based on manufacturing specifications with the applied internal loads described in Appendix F. The applied internal loads are normalized for fatigue life purposes. The maximum stresses due to tension and torsion loading will be constant around the circumference of the shaft and bending stresses will be a maximum at only one location. Figure 10.6 shows the ANSYS solution for the

normal stress distribution along the z-axis. Because of the imposed boundary conditions only a small section of the drag beam in the vicinity of the fillet radius was necessary to gain better insight into the stress distribution. Figures 10.7 and 10.8 show the normal and first principal stress distribution in the critical section of the drag beam. It can be shown from Figure 10.8 that careful attention must be given to the applied boundary and loading conditions. The stress distribution of the first principal stress is a maximum at a location affected only by the applied loading. This issue will be further addressed in the fatigue life analysis.

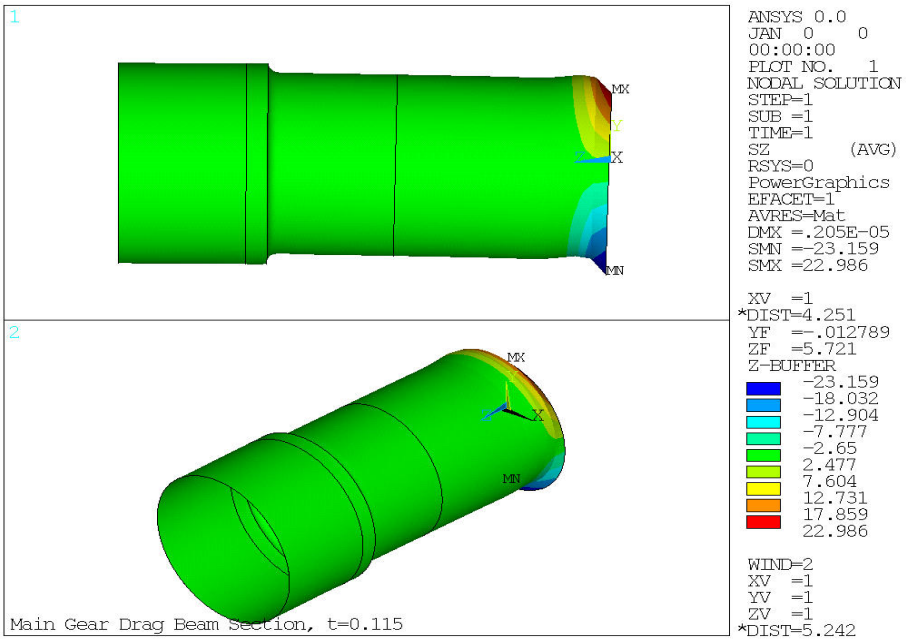

Figure 10.6 – Drag Beam Normal Axial Stress Distribution, (psi)

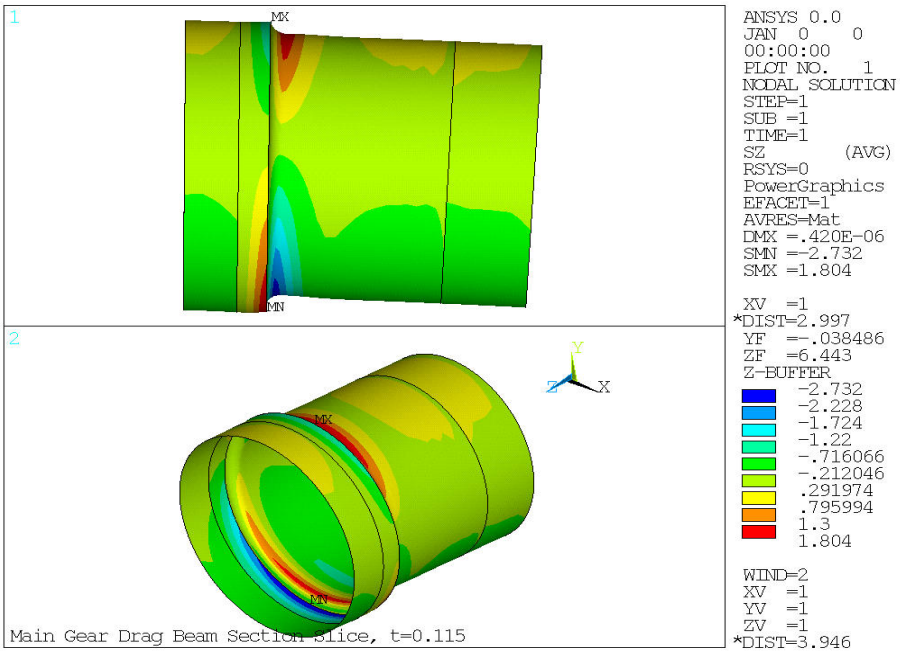

Figure 10.7 – Drag Beam Normal Stress Distribution in the Critical Section, (psi)

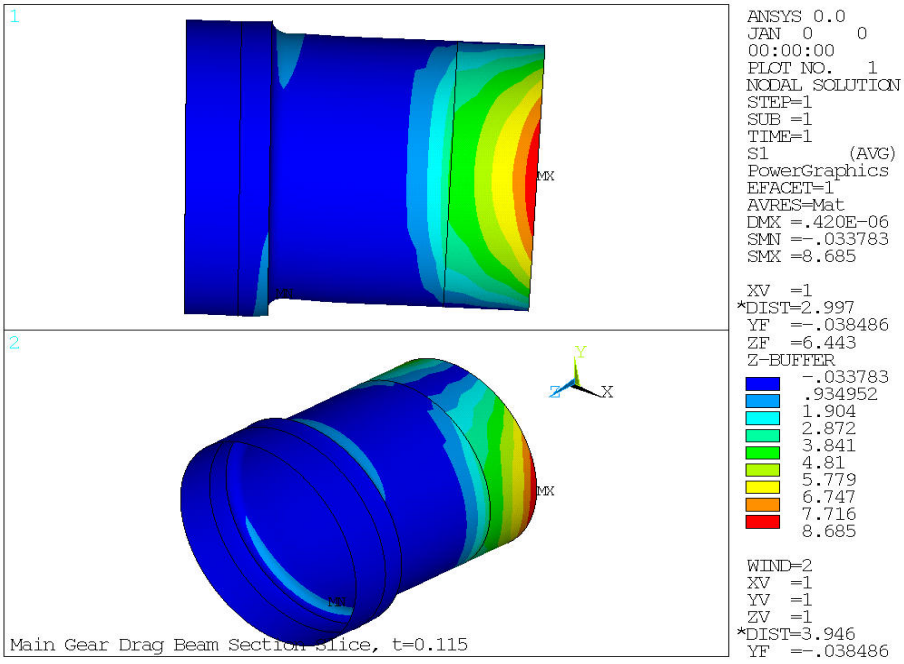

Figure 10.8 – Drag Beam First Principal Stress Distribution in the Critical Section, (psi)

In references [4, 23, 24], Draper discusses the effects of stress gradients and notch sensitivity on total fatigue life and fatigue life to crack initiation. Stress gradients can have an important effect on the total fatigue life (crack initiation plus propagation). As the radius of a blunt notch is reduced, the shape of the groove approaches that of a crack. From LEFM (discussed in Section 3.4) a crack will not propagate when ΔK is less than the threshold fracture mechanics parameter ΔK_{th}. Therefore, the endurance limit stress for a crack is the threshold value of ΔS. However, experimental evidence has shown that when considering crack initiation only fatigue strength reduces with increasing stress concentration. Thus, crack initiation depends on surface strains and stresses and it is not affected by stress gradients.

Since the stress gradient can typically be ignored in fatigue analysis, local strains are the dominant factor. For this reason, the drag beam was sectioned into three material groups with each group consisting of equivalent material properties. This allowed a fatigue analysis to be conducted only at the fillet section of the drag beam.

Typically a component with multiple applied loads would be modeled such that a FE analysis would be used to calculate the unit load stress tensor for each applied load separately. In ANSYS this would equate to multiple load cases in the FE analysis. For this research, it was assumed that each applied load experienced identical load histories in both stress amplitude and frequency. Therefore, the force boundary conditions from Table 10.2 can be normalized with respect to the bending moment, applied as a single load case, and scaled by the load history in Table 10.1. The LDF file of the load history used for this analysis is shown in Appendix H. Based on Draper's[4, 6, 23, 24] work and the results from the

fatigue analysis of the flat plate describe previously, the Brown-Miller-Morrow fatigue algorithm was used. The nodal fatigue life contours of the main gear drag beam with a wall thickness of 0.115 inches are shown Figure 10.9. The hot spots are located at the fillet radius on both the upper and lower surface of the drag beam. These locations are expected since the dominant load is the applied bending moment about the x-axis. The first nodal contour plot in Figure 10.9 has been rotated 90 degrees to provide a better view of the critical area of the lower surface.

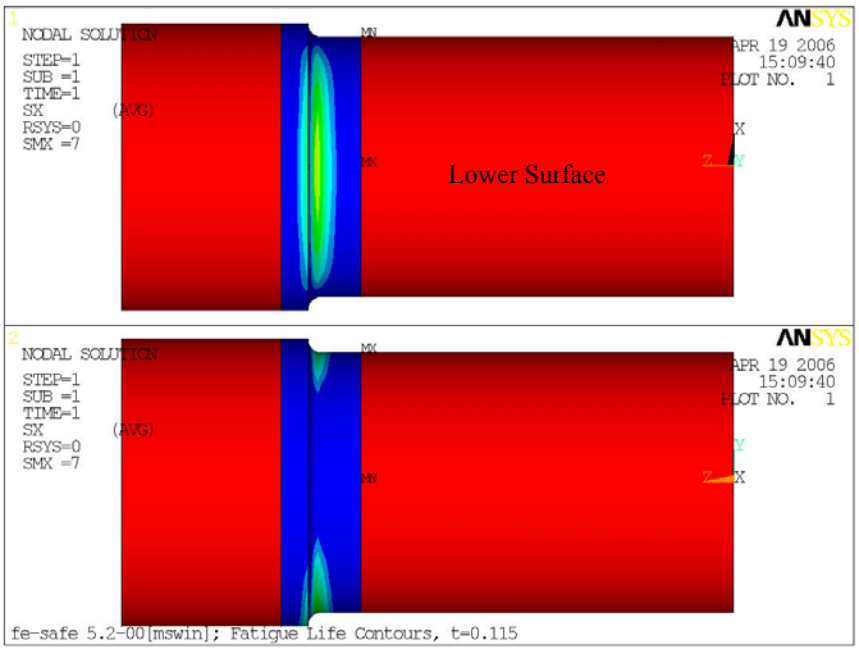

Figure 10.9 – Nodal Fatigue Life Contours, t = 0.115 inches

The fatigue analysis log (Appendix I) shows that the worst-case life for the main gear drag beam is 1324 repeats of the fatigue loading cycle occurring at 3160.6 which equates to element 3160, node 6. Node 6 coincides with the global node 3168. When using shell elements, the fatigue life results values are written to the ANSYS elemental variable Sx.

Thus, in order to view fatigue life values in the ANSYS results viewer, elemental contour plots should be observed. Figure 10.10 shows the elemental fatigue life contours with a $\log_{10}$ scale and an enlarged view of the critical area. The areas in red have been "turned off" during the fatigue analysis since, as stated earlier, the fillet radius is the critical area and to ensure boundary and loading conditions will not interfere with the fatigue life analysis. The areas in blue have a fatigue life value of 7, which in a $\log_{10}$ scale equates to 10000000 repeats or an infinite life. Element 3160 has a fatigue life value of 3.12 which equates to 1324 repeats of the fatigue loading history. Additionally, one repeat of the load history represents 1000 flight hours, therefore 1324 repeats of the drag beam with an initial wall thickness of 0.115 inches essentially gives an infinite life of 1,324,000 flight hours.

The location of the shortest-life occurs at the lower surface on the inner wall of the drag beam. A stress analysis alone determined that the location of the maximum normal stress in the axial direction and the maximum principal stress occur at the upper surface on the outer diameter. The dominant applied load is the bending moment; therefore the fluctuating load history cycles both the upper and lower surfaces of the drag beam in tension and compression. Thus, with the addition of the applied axial load, it is feasible that the maximum damage would occur on the lower surface, where the inner diameter is under tension and the outer diameter is under compression.

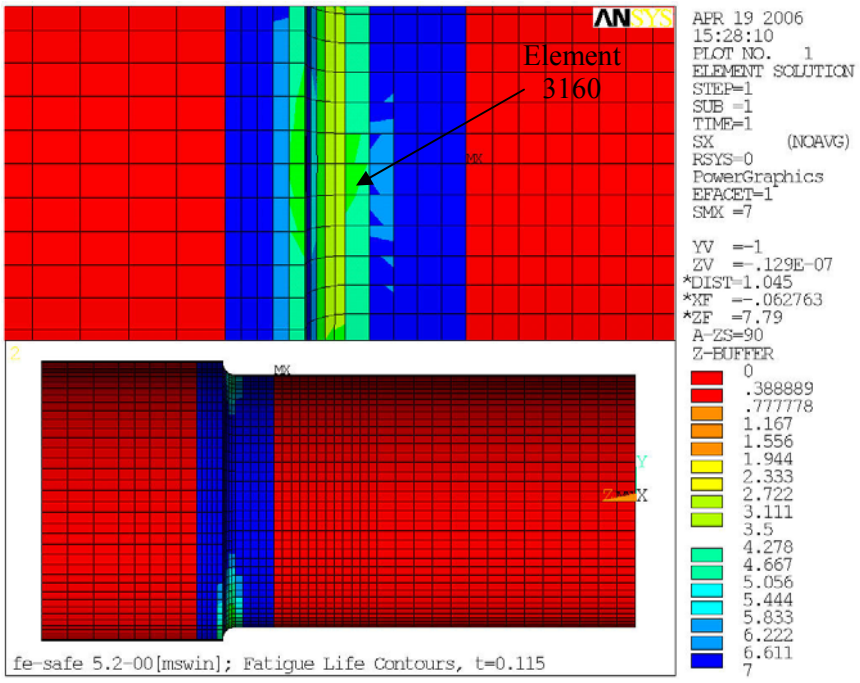

Figure 10.10 – Elemental Fatigue Life Contours in Log_{10} Scale, t = 0.115 inches

Since the goal of this research is to analyze and predict the service life of an illustrative complex aircraft component and determine if a reworked part is suitable for continued service, the effects of wall thickness reduction on fatigue life was conducted. The purpose of this comparison was to evaluate the effect of removing surface corrosion. The depth of surface corrosion is typically measured in **m**m, and according to the FAA "the standard procedure for corrosion removal is by hand sanding with mild abrasive mats, cloths, and papers, such as fine aluminum oxide grit. The use of power tools and chemical corrosion removers is considered undesirable" [57]. For this research it was assumed that a reduction in the thickness of the landing gear would be uniform throughout the inner surface and material removal would be in increments of 0.005 inches. Table 10.4 compares the calculated time to crack initiation for the predicted fatigue life using fe-safe for several

values of the wall thickness. It can be seen that with an initial reduction in the wall thickness from 0.115 to 0.110 inches or 4.35%, the calculated fatigue life is reduced from 1324 to 702 repeats, or a 46.98% reduction in fatigue life. Additionally, a 13.0% reduction in the wall thickness results in a reduction in the calculated fatigue life by 87.54%. For all simulations, the location of the crack initiation remained at element 3160. Figures 10.11 and 10.12 show the nodal and elemental fatigue life contours of the main gear drag beam with a wall thickness of 0.100 inches, respectively. Figure 10.12 also gives an enlarged view of the critical area where element 3160 has a fatigue life value in a $\log_{10}$ scale of 2.21, which is equivalent to 165 repeats of the applied load history. The predicted crack initiation was located on the lower inner surface of the drag beam.

Table 10.4 – Comparison of Predicted Fatigue Life with Varying Thickness

Shaft thickness (inches)	Load History Repeats	Elemental Crack Initiation Location
0.115	1324	3160
0.110	702	3160
0.105	372	3160
0.100	165	3160

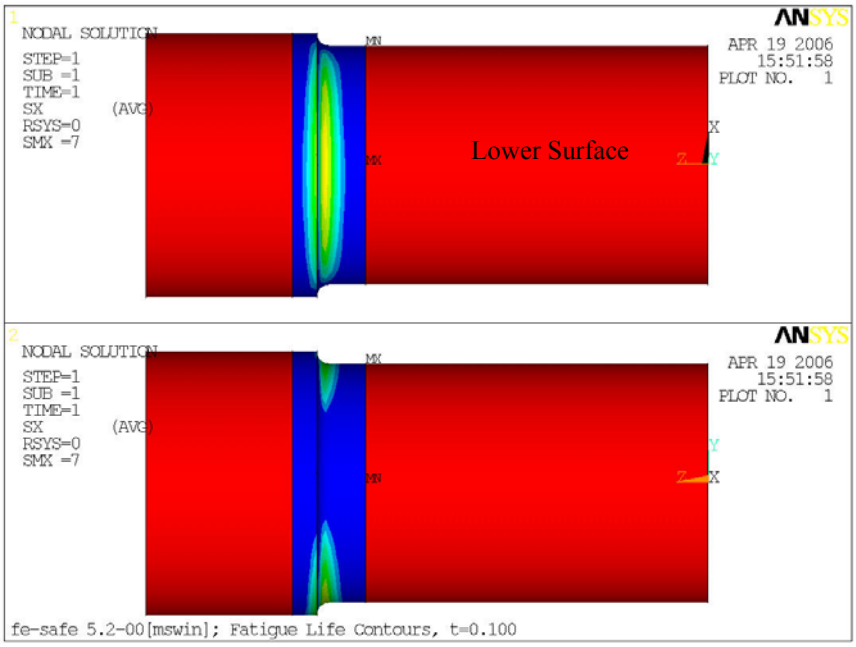

Figure 10.11 – Nodal Fatigue Life Contours, t = 0.100 inches

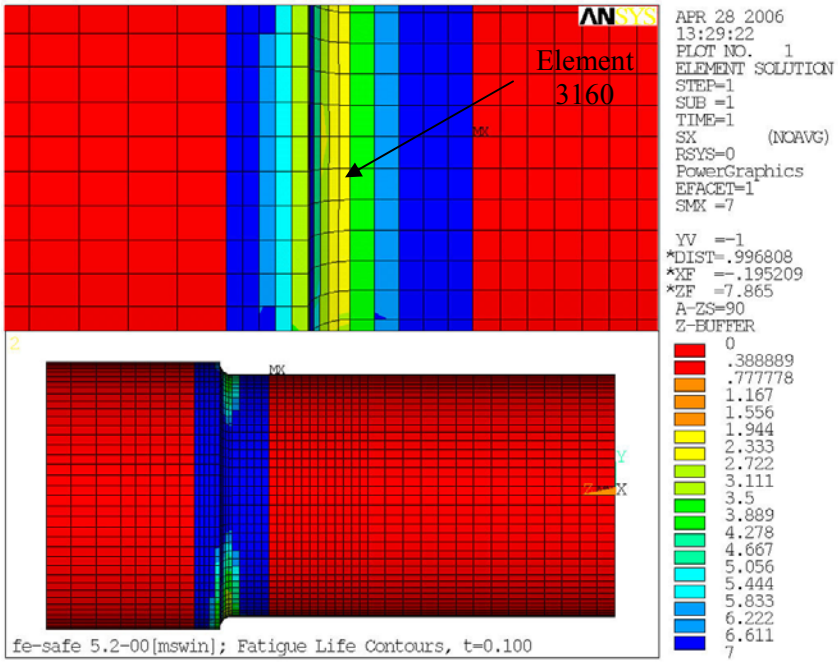

Figure 10.12 – Elemental Fatigue Life Contours in Log_{10} Scale, t = 0.100 inches

10.6 Merit of Numerical Solutions

Confidence in the numerical results presented in this thesis was gained by comparing fatigue lives of an isotropic flat plate with a central located hole under both constant and variable amplitude loading with previously published experimental results. In this case, excellent agreement was achieved. In addition, several fatigue algorithms currently used for life prediction were compared. Empirical validations of the numerical results for the main gear drag beam compared to what is found during actual maintenance procedures were limited. Minimal information was published with regards to the effect of material removal on predicted fatigue life. However, with the confidence gained in the accuracy and precision of the flat plate, the simulated results of the predicted fatigue life of the drag beam do provide insight into the time-to-crack initiation and its corresponding location.

11 CONCLUSIONS AND RECOMMENDATIONS FOR FUTURE WORK

11.1 Conclusions

The main goal of this work was to develop a practical fatigue analysis methodology for life prediction of rotary-wing aircraft components. The focus of this fatigue capability was to gain insight into the current life prediction methodologies and their use. A critical issue facing engineers is the timely scheduling of maintenance and its effect on fatigue life. Therefore, it was demonstrated that commercially available fatigue software can be used to gain an understanding of the effects of repairs on the continued use of parts in service.

This research has shown that with commercially available software codes, predicted fatigue life on aircraft components can be performed with reasonable accuracy and efficiency. This was demonstrated with the predicted fatigue life of the flat plate under variable amplitude loading. Although this is a relatively simple geometry with widely published results, it provided insight into the capabilities of current fatigue and durability software. In addition, the computational time was minimal with an analysis time under 25 minutes even when the applied loading consisted of 161,034 cycles. The numerical simulations for this classical model also helped to reiterate the many pitfalls that may occur when conducting a life prediction analysis. In addition to accurate applied loadings, accurate material properties are essential (shown in Table 9.2), as well as the correct use of the stress and strain life algorithms, with and without mean stress correction.

This research has also shown that the potential to predict the service life of aircraft components in a timely manner and to determine if reworked parts are suitable for continued service is possible. An illustrative helicopter main gear drag beam was analyzed and the

effects on fatigue life by reducing the thickness implied that preventative maintenance scheduling can be achieved.

11.2 Recommendations for Future Work

Future work needs to be performed in several key areas. The progression of the drag beam section to include the entire drag beam should be performed. The continued development and simulation on the effects of current maintenance procedures to remove corrosion and its possible redistribution of critical areas need to be investigated further. A more detailed understanding of the applied load history as well as an investigation into the capabilities of the fatigue and durability software to incorporate the effects of multiple loads not in phase should be performed. Additionally, an investigation into the predicted fatigue life of an illustrative aircraft component with in-flight data should also be conducted to further validate this procedure for general use in life prediction of critical aircraft components.

12 REFERENCES

[1] Liao, M., Bellinger, N., Komorowski, Jerzy P., "Analytical Methodologies for Fatigue Life Prediction of Corroded Fuselage Splices," *Proceedings of the 8th Joint FAA/DoD/NASA Conference on Aging Aircraft*, Palm Springs, CA, January 2005.

[2] Hoffman, Margery E., Hoffman, Paul C., "Corrosion and Fatigue Research – Structural Issues and Relevance to Naval Aviation," *International Journal of Fatigue*, Vol. 23, Sup. 1, pp. S1-S10, 2001.

[3] Everett, Richard A. Jr., "Crack-Growth Characteristics of Fixed- and Rotary-Wing Aircraft," *Proceedings of the 6th Joint FAA/DoD/NASA Conference on Aging Aircraft*, San Francisco, CA, September 2002.

[4] Draper, John, Modern Metal Fatigue Analysis, Safe Technology Limited, Sheffield UK, 2004.

[5] Newman, J. C. Jr., "Advances in Fatigue and Fracture Mechanics Analyses for Metallic Aircraft Structures," NASA TM-2000-210084, 2000.

[6] Draper, J., Aveline, R., "How to Achieve Valid Results in Durability Analysis from ANSYS," Proceedings of the ANSYS International User's Conference, Pittsburgh USA, 2004.

[7] Everett, Richard A. Jr., "A Comparison of Fatigue Life Prediction Methodologies for Rotorcraft," *Journal of the American Helicopter Society*, Vol. 37, No. 2, pp. 54-60, April 1992.

[8] Everett, Richard A. Jr., Bartlett, Felton D. Jr., Elber, Wolf, "Probabilistic Fatigue Methodology for Safe Retirement Lives," *Journal of the American Helicopter Society*, Vol. 37, No. 2, pp. 41-53, April 1992.

[9] Newman, J. C. Jr., "Crack Closure Model for Predicting Fatigue Crack-Growth under Aircraft Spectrum Loading," ASTM STP 748, American Society of Testing and Materials, Philadelphia, 1981, pp 53-84.

[10] Newman, J. C. Jr., Phillips, E.P., Swain, M. H., "Fatigue-Life Prediction Methodology using Small-Crack Theory," *International Journal of Fatigue*, Vol. 21, Issue 2, 1999, pp. 109-119.

[11] Newman, J. C. Jr., Phillips, E. P., Everett, R. A. Jr., "Fatigue Analyses Under Constant Amplitude- and Variable Amplitude Loading Using Small-Crack Theory," NASA/TM-1999-209329, 1999.

[12] Newman, J. C. Jr., Irving, P. E., Lin, J., Le, Dy, "Crack-Growth Predictions in a Complex Helicopter Component Under Spectrum Loading", *Proceedings of the 8th Joint FAA/DoD/NASA Conference on Aging Aircraft*, Palm Springs, CA, January 2005.

[13] Newman, J.C. Jr., "FASTRAN II – A Fatigue Crack Growth Structural Analysis Program," NASA TM 104159, 1992.

[14] NASGRO – Fracture Mechanics and Fatigue Crack Growth Analysis Software. http://www.nasgro.swri.org

[15] AFGROW - http://afgrow.wpafb.af.mil

[16] Everett, R. A. Jr., Newman, J. C. Jr., Phillips, P., "The Effects of a Machining-Like Scratch on the Fatigue Life of 4340 Steel," *Journal of the American Helicopter Society*, Vol. 45, No. 3, pp. 151-155, July 2000.

[17] Merati, Ali, "A Study of Nucleation and Fatigue Behavior of an Aerospace Aluminum Alloy 2024-T3," *International Journal of Fatigue*, Vol. 27, Issue 1, 2005, pp. 33-44.

[18] Adey, Robert A., Baynham, John M. W., Mellings, Sharon, Curing, Tom, "Fatigue Life and Crack Growth Prediction Using FEM Data," Computational Mechanics Inc., BEASY, 2003. http://www.beasy.com

[19] Conle, F. A., Chu, C.-C., "Fatigue Analysis and the Local Stress-Strain Approach in Complex Vehicular Structures," *International Journal of Fatigue*, Vol. 19, Supp. No. 1, 1997, pp. S317-S323.

[20] Chu, C.-C., "Mulitaxial Fatigue Life Prediction Method in the Ground Vehicle Industry," *International Journal of Fatigue*, Vol. 19, Supp. No. 1, 1997, pp. S325-S330.

[23] Draper, John, "Metal Fatigue – Failure and Success," Les Methodes de Dimensinnement en Fatigue, Journee Scientifique, 2004.

[24] Mercer, I., Malton, G., Draper, J., "Investigating Fatigue Failures using Analysis and Testing – some do's and don'ts," Proceedings of the ABAQUS International User's Conference, Germany, 2003.

[25] Colquhoun, C., Draper, J., "Fatigue Analysis of an FEA Model of a Suspension Component, and Comparison with Experimental Data," Proceedings NAFEMS Conference 'Fatigue Analysis from Finite Element Models', Wiesbaden Germany, 2000.

[26] Hughes, A., Draper, J., Kemp, M.., "Fatigue Assessment of an Oilpan Incorporating Manufacturing Effects," 'Engineering Integrity', *The Journal of the Engineering Integrity Society*, January 2002.

[27] Safe Technology Limited, "fe-safeWorks version 5 – Durability Analysis Suite from Safe Technology," Sheffield UK, 2005. http://www.safetechnology.com

[28] Bannantine, Julie A., Comer, Jess J., Handrock, James L., Fundamentals of Metal Fatigue Analysis, Prentice-Hall, Inc., New Jersey, 1990.

[29] Dowling, Norman E., Mechanical Behavior of Materials, Second Edition, Prentice-Hall, Inc., New Jersey, 1999.

[30] Sanford, R. J., Principles of Fracture Mechanics, Pearson Education, Inc., New Jersey, 2003.

[31] Suresh, S., Fatigue of Materials, Second Edition, University Press, Cambridge, United Kingdom, 1998.

[32] Pilkey, Walter D., Peterson's Stress Concentration Factors, Second Edition, John Wiley & Sons, Inc., New York, 1997.

[33] Smith, K.N., Watson, P., Topper, T.H., "A Stress-Strain Function for the Fatigue of Metals," Journal of Materials, ASTM, Vol. 5, No. 4, 1970, pp. 767-778.

[34] Downing, S. D., Socie, D. F., "Simplified Rainflow Counting Algorithms," *International Journal of Fatigue,* Vol. 4, No. 1, 1982, pp. 31-40.

[35] Rice, R.C. (ed.), Fatigue Design Handbook, 3rd ed., SAE Pub. No. AE-22, Society of Automotive Engineers, Warrendale, PA, 1997.

[36] Palmgren, A., Ball and Roller Bearing Engineering Third Edition, translated by Gunnar Palmgren and Allan Palmgren, SFK Industries, Inc., Philadelphia, PA, 1956.

[37] Miner, M.A., "Cumulative Damage in Fatigue," *Journal of Applied Mechanics*, ASME, Vol. 12, September 1945.

[38] Madayag, A.F. (ed.), Metal Fatigue: Theory and Design, Wiley, New York, 1969.

[39] Edwards, P.R., Darts, J., "Standardised Fatigue Loading Sequences for Helicopter Rotors," *Part 1: Background and Fatigue Evaluation, Part 2: Final Definition of Helix and Felix*, National Aerospace Laboratory NLR, The Netherlands, NLR TR 81043 U.

[40] Bannantine, J.A., Socie, D.F., "A Variable Amplitude Multiaxial Fatigue Life Prediction Method," *Fatigue Under Biaxial and Multiaxial Loading*, European Structural Integrity Society, ESIA Publication 10, Mechanical Engineering Publications, London, 1991, pp. 35-51.

[41] Socie, D.F., Marquis, G.B., Multiaxial Fatigue, Society of Automotive Engineers, Inc., Warrendale, PA, 2000.

[42] Kandil, F. A., Brown, M. W., Miller, K. J., "Biaxial Low-Cycle Fatigue Fracture of 316 Stainless Steel at Elevated Temperatures," Book 280, The Metals Society, London, 1982, pp. 203-210.

[43] Fatemi, A., Socie, D. F., "A Critical Plane Approach to Mulitaxial Fatigue Damage Including Out-of-Phase Loading," *Fatigue and Fracture of Engineering Materials and Structures*, Vol. 11, No. 3, 1988, pp. 149-166.

[44] Wang, C.H., Brown, M.W., "A Path-Independent Parameter for Fatigue Under Proportional and Nonproportional Loading," *Fatigue and Fracture of Engineering Materials and Structures*, Vol. 16, No. 12, 1993, pp. 1285-1298.

[45] Chu, C.-C., Conle, F. A., Bonnen, J.F., "Multiaxial Stress-Strain Modeling and Fatigue Life Prediction of SAE Axle Shafts," *Advances in Multiaxial Fatigue*, ASTM STP 1191, American Society for Testing and Materials, PA, 1993, pp.37-54.

[46] McDiarmid, D.L., "A General Criterion for High Cycle Multiaxial Fatigue Failure," *Fatigue and Fracture of Engineering Materials and Structures*, Vol. 14, No. 4, 1991, pp. 429-453.

[47] Dang Van, K., "Macro-Micro Approach in High-Cycle Multiaxial Fatigue," *Advances in Multiaxial Fatigue*, ASTM STP 1191, D.L. McDowell, R. Ellis, eds., American Society for Testing and Materials, West Conshohocken, PA, 1993, pp. 120-130.

[48] Conle, A., Topper, T.H., "Overstrain Effects During Variable Amplitude Service History Testing," *International Journal of Fatigue*, Vol. 2, No. 3, 1980, pp. 130-136.

[49] ANSYS, Inc., Modeling Software, *ANSYS 9.0 Documentation*, 2004. http://www.ansys.com

[50] ASM Aerospace Specification Metals Inc. http://www.aerospacemetals.com

[51] Draper, J., Mercer, Ian, Personal Correspondence, February to March 2006.

[52] Genesis for Fatigue, GENErator for StandardIsed Sequences for Fatigue, National Aerospace Laboratory – the Netherlands.
http://www.nlr.nl

[53] Hertzberg, R. W., Deformation and Fracture Mechanics of Engineering Materials, 4th Edition, John Wiley & Sons, Inc., New York, 1995.

[54] Kinzie, Richard, "USAF Cost of Corrosion," *Proceedings of the 8th Joint FAA/DoD/NASA Conference on Aging Aircraft*, Presentation, Palm Springs, CA, January 2005.

[55] Kovaleski, Kevin, "Progress in NAVAIR's Corrosion Fleet Focus Team," *Proceedings of the 8th Joint FAA/DoD/NASA Conference on Aging Aircraft*, Presentation, Palm Springs, CA, January 2005.

[56] Integrated Publishing
http://www.tpub.com

[57] Advisory Circular, "Acceptable Methods, Techniques, and Practices – Aircraft Inspections and Repair," *US DoT/FAA*, AC 43.13-1B, September, 1998.

13 APPENDICES

Appendix A – Materials Data File Created for Use Within Fe-Safe

Detailed in this section is the material data file created using material properties published by Everett[7,8]. The created 4340 steel was used for all simulations pertaining to the flat plate.

SAFE TECHNOLOGY LTD MATERIAL DEFINITION FILE

NOTES -9999 indicates a parameter is not set !!!
All items after a # are comments that will be ignored.

MATERIAL-NAME
Everett-SAE-4340
MATERIAL-CLASS
Steel (Ductile)
ALGORITM
BrownMiller:-Morrow
DISPLAY-UNITS
Metric - MPa, deg.C
DATA-SOURCE
SN curve derived from Sf' and b
DATA-QUALITY
None

COMMENT-1
Alloy Steel AISI4340 STEEL
COMMENT-2
Copied from SAE-4340
REVISION-NUMBER
110
REVISION-DATE
Tue Mar 07 11:58:58 2006

REVISION-HISTORY
None
CONSTANT-AMPLITUDE-ENDURANCE-LIMIT(2nf)
2e+007
TEMPERATURE-LIST(deg.C)
0
STRAIN-RATE-LIST(1/Hr)
1
POISSONS-RATIO

0.3
YOUNGS-MODULUS(MPa)
206843
0.2%-PROOF-STRESS(MPa)
1172
ULTIMATE-TENSILE-STRENGTH(MPa)
1462
ULTIMATE-COMPRESSIVE-STRENGTH(MPa)
-9999
K'-TENSILE-CYCLIC
2130
n'-TENSILE-CYCLIC
0.15
K'-COMPRESSIVE-CYCLIC
-9999
n'-COMPRESSIVE-CYCLIC
-9999
SECANT-SLOPE-COMPRESSIVE-CYCLIC
-9999
SECANT-SLOPE-TENSILE-CYCLIC
-9999
MODULUS-OF-UNLOADING
-9999
K-MONOTONIC
-9999
n-MONOTONIC
-9999
damage-to-Harden(0->1)
0
ef'-STRAIN-LIFE-CURVE
0.48
c-STRAIN-LIFE-CURVE
-0.6
Sf'-STRAIN-LIFE-CURVE
1999
b-STRAIN-LIFE-CURVE
-0.091
b2-STRAIN-LIFE-CURVE
-9999
2nf-ABOVE-WHICH-b2-IS-USED
-9999
S-N-CURVE
Nf S(MPa)
1.336E3 1206

7.306E3 827
3.406E4 552
6.136E4 483
9.728E4 448
1.168E5 413
2.577E6 379
3.757E6 362
5.993E6 345
COEFF-SWT-CAST-IRON-LIFE-CURVE
-9999
EXPONENT-SWT-CAST-IRON-LIFE-CURVE
-9999
BF-PROBABILITY
3
QMUF-PROBABILITY
0.25
IN-PHASE-THERMAL-FACTOR
-9999
OUT-OF-PHASE-THERMAL-FACTOR
-9999
CREEP-ENDURANCE-LIMIT(2nf)
2e+007
CREEP-TEMPERATURE_THRESHOLD(deg.C)
300

Appendix B – Load Definition File used for Constant Amplitude Loading Analysis

```
Con Amp unit Load R=0.txt
1
0



#
# Constant Amplitude Loading for Everett model with R=0
# Applied Gross-Section Load is varied by changing the scale factor
# 37.5 39.375 41.25 45.0 48.75 52.5 60.0 90.0 131.25 (ksi)
#

BLOCK n=1, SCALE=37.5
ds=1, lh=C:\Program Files\fesafe\version.5.1-02\data\Con Amp unit Load R=0.txt, signum=1
END
```

Appendix C – Fe-safe Output File for Constant Amplitude Loading

Setting output filename as defined in command line parameter o, to:
c:\data\fesafe\CAL_30000v0.3_BMM_50.rst
Setting material to Everett-SAE-4340 in database C:\Program Files\fesafe\version.5.1-02\local\JMC_Materials.dbase
Checking C:\Program Files\fesafe\version.5.1-02\database\system.dbase
Checking C:\Program Files\fesafe\version.5.1-02\database\dangvan.dbase
Checking C:\Program Files\fesafe\version.5.1-02\database\AFS_Cast_Iron.dbase
Checking C:\Program Files\fesafe\version.5.1-02\local\local.dbase
Checking C:\Program Files\fesafe\version.5.1-02\local\JMC_Materials.dbase
Found database
Checking Everett-4340
Checking Everett-SAE-4340
Material set OK.

Reading LDF file C:\Program Files\fesafe\version.5.1-02\data\Cons Amp Loading-Everett (ksi).ldf
BLOCK n=1, SCALE=37.5
ds=1, lh=C:\Program Files\fesafe\version.5.1-02\data\Con Amp unit Load R=0.txt, signum=1
END
End of read LDF file C:\Program Files\fesafe\version.5.1-02\data\Cons Amp Loading-Everett (ksi).ldf

Starting Analysis ...
FATIGUE LIFE : 5.1-02 fe-safe[mswin]
Copyright Safe Technology 1996-2005

Algorithm	BrownMiller:-Morrow
Material	Everett-SAE-4340-JMC_Materials.dbase
Surface	Mirror Polished - Ra <= 0.25 um-default.kt
Kt	1
UTS	1462 MPa
Model File (s)	C:\Program Files\fesafe\version.5.1-02\data\Ansys\30000v-0.3.rst
FEA Units	S=ksi e=strain T=deg.C
Loading	Loading is equivalent to 1 Repeats
	Load Definition File : Cons Amp Loading-Everett (ksi).ldf
	Elastic FEA
Scale factor	37.5
Overflow Life value	0
Infinite Life value	Material CAEL
Temperature analysis	Enabled if temperatures present
Histories	None

```
Log                   None
List of Items         None
Histories for Items   None
Log for Items         None
Output contours to    c:\data\fesafe\CAL_30000v0.3_BMM_50.rst
Contour variables      LOGLife-Repeats,
....Intermediate      c:\safeResultsArchive\fesafe.fer
Influence coeffs.     Disabled
Gauges.               Disabled

D'set  Step   Inc   T/Freq  Type        Pos    Number      What  Direct
   1     1     1      1.0     S   Elemental       600  elements  3 -> -1

D'set                  Shear  File              Description
   1                0 -> -1  30000v-0.3.rst       Everett Unit Load, E=30000 (ksi) v=0.3

  %      Time       Life-Repeats
 100    0:00:00     1829361@599.3          600 of 600

Summary
=======
Worst Life-Repeats                  : 1829360.875
  at Element 599.3
Analysis time                       :   0:00:00
 Fatigue Analysis Completed.
DLL mode ...
ansys_io.dll/.sl version 5.1-03
Interface to ANSYS .rst datafiles
Copyright Safe Technology 1996-2005

Source file       : C:\Program Files\fesafe\version.5.1-02\data\Ansys\30000v-0.3.rst
ANSYS Output      : c:\data\fesafe\CAL_30000v0.3_BMM_50.rst
Results File : c:\safeResultsArchive\fesafe.fer
  contains   : LOGLife-Repeats
From ANSYS version :  9.0
Exporting set : 1
 Variable     : LOGLife-Repeats
  as          : Sx
  Header updated, adding element data.
Results handler intelligent sorting 'CRESHND_SORT=2', there are too few items for a pre-
sort to be beneficial
ANSYS writer (dll) completed
Time in module : 0:00:00
DLL mode done
```

Appendix D – Load Definition File used for Variable Amplitude Loading

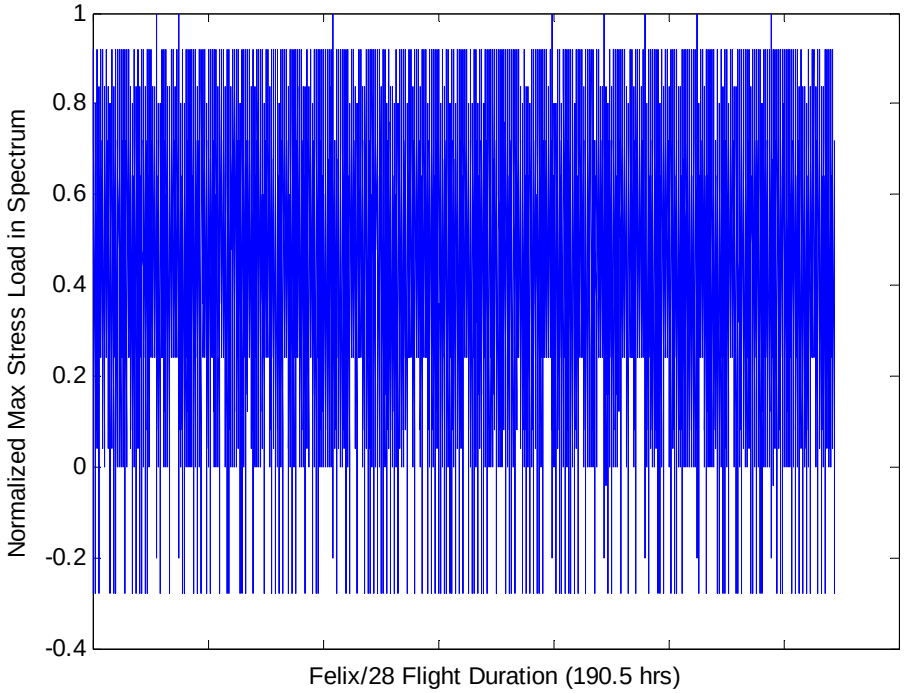

Figure 11.1 – Felix/28 spectrum consisting of 161,034 cycles

```
#
# Variable Amplitude Loading from Felix/28 for Everett model
# Applied Gross-Section Load is varied by changing the scale factor
# 37.5 39.375 41.25 45.0 48.75 52.5 60.0 90.0 131.25 (ksi)
#

BLOCK n=1, SCALE=37.5
ds=1, lh=C:\Program Files\fesafe\version.5.1-02\data\Felix28_stresses_max1.txt, signum=1
END
```

Appendix E – Hand Calculations utilizing the Stress Life Approach

Free Body Diagram of the Main Gear Drag Beam:

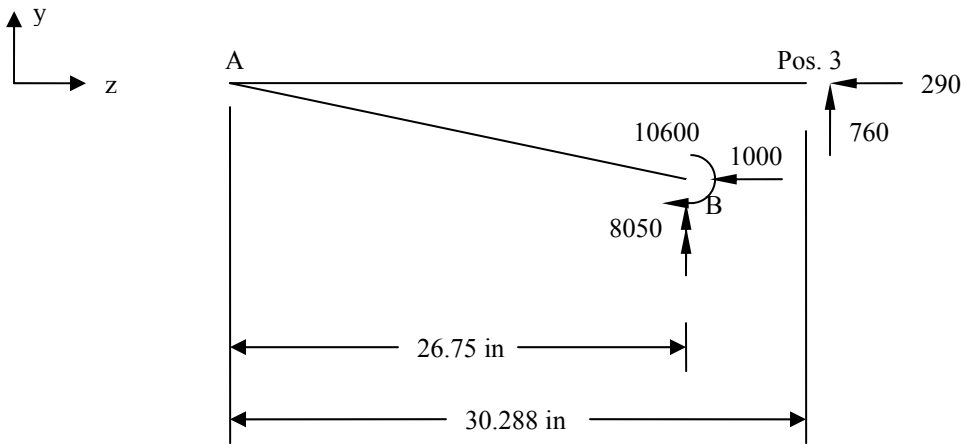

$D_o = 5.00\ in$
$D_i = 4.77\ in$

$A = 1.765 in^2$

$$I_{XX} = I_{YY} = \frac{\pi}{4}\left(r_o^4 - r_i^4\right) = 5.267 in^4$$

Resolve loads in Drag Beam Axes:
(loads in *lbs*)

$$F_{y-1000} = 1000\left(Sin\left(26^o 51'\right)\right) = 452$$
$$F_{z-1000} = 1000\left(Cos\left(26^o 51'\right)\right) = 892$$
$$T = 8050\left(Sin\left(26^o 51'\right)\right) = 3636$$
$$M_{xx} = 8050\left(Sin\left(26^o 51'\right)\right) = 7182$$

Determination of stresses at section A:

$$F_Z = 892 + 290 = 1182 \rightarrow compression$$
$$T = 3636 \rightarrow tension$$
$$M_{XX} = 7182 \rightarrow tension$$
$$M_{YY} = -452(26.75) - 10600 + 706(30.288) = 1308 \rightarrow compression$$
$$M_{RES} = \sqrt{(M_{XX})^2 + (M_{YY})^2} = \sqrt{(7182)^2 + (1308)^2} = 7300$$

Normal Stress:

$$\sigma_Z = \frac{F_Z}{A} + \frac{M_{RES}(c)}{I} = \frac{1182}{1.765} + \frac{7300(2.5)}{5.267} = 4134\,psi$$

Shear Stress:

$$\tau_{XY} = \frac{T(c)}{J} = \frac{3636(2.5)}{2(5.267)} = 863\,psi$$

Amplitude and Mean Stresses (R = 0):

$$\sigma_{za} = \sigma_{zm} = \frac{\sigma_Z}{2} = \frac{4134}{2} = 2067\,psi$$

$$\tau_{xya} = \tau_{xym} = \frac{\tau_{XY}}{2} = \frac{863}{2} = 431.5\,psi$$

Effective Stress Amplitude: From Eq. (39)

$$\tilde{\sigma}_a = \frac{1}{2}\sqrt{(\sigma_{xa} - \sigma_{ya})^2 + (\sigma_{ya} - \sigma_{za})^2 + (\sigma_{za} - \sigma_{xa})^2 + 6(\tau_{xya}^2 + \tau_{yza}^2 + \tau_{zxa}^2)}$$

$$\tilde{\sigma}_a = \frac{1}{2}\sqrt{(0-0)^2 + (0-2067)^2 + (2067+0)^2 + 6(431.5^2)} = 1554\,psi$$

Effective Mean Stress: From Eq. (40)

$$\tilde{\sigma}_m = \sigma_{xm} + \sigma_{ym} + \sigma_{zm}$$

$$\tilde{\sigma}_m = 0 + 0 + 2067 = 2067\,psi$$

Equivalent Completely Reversed Uniaxial Stress: From Eq. (41)

$$\sigma_{ar} = \frac{\tilde{\sigma}_a}{1 - \frac{\tilde{\sigma}_m}{\sigma_f'}} = \frac{1554}{1 - \frac{2067}{436550}} = 1561\,psi$$

Estimated Fatigue Life: From Eq. (3)

$$N_f = \frac{1}{2}\left(\frac{\sigma_{ar}}{\sigma_f'}\right)^{\frac{1}{b}} = \frac{1}{2}\left(\frac{1561}{436550}\right)^{\frac{1}{-0.101}} = \infty$$

Where material constants $\sigma_f^{'}$ and b are from Table 10.3. This method can be implemented for each block within a variable amplitude loading to reduce a complex state of stress into a uniaxial state of stress. The life in repetitions to failure may then be estimated from the *n* and N_f values using the Palmgren-Miner rule, equation (36).

With the use of the S-N curve from Figure 10.3 and the typical load history given in Table 10.1, the predicted fatigue life can be determined. Each vibratory stress amplitude is applied for a number of cycles, n_1, where the number of cycles to failure from the S-N curve for block 1 is $N_{f1.}$ The damage is the fraction of the life used, n_1/N_{f1}. The Mean-Life in damage per 1000 hours is then:

$$B_f = \frac{1}{\left[\Sigma \frac{n_j}{N_{fj}}\right]}$$

$$B_f = \frac{1}{\left[\left(\frac{190}{\infty}\right)+\left(\frac{190}{\infty}\right)+\left(\frac{190}{240000}\right)+\left(\frac{190}{7000000}\right)+\left(\frac{150}{\infty}\right)+\ldots+\left(\frac{1}{\infty}\right)\right]} = 0.00763$$

$$MeanLife = \frac{1000\,flightHours}{0.00763} = 131060\,Hrs$$

Appendix F – Determination of Internal Loads of the Main Gear Drag Beam

Free Body Diagram of the Main Gear Drag Beam:

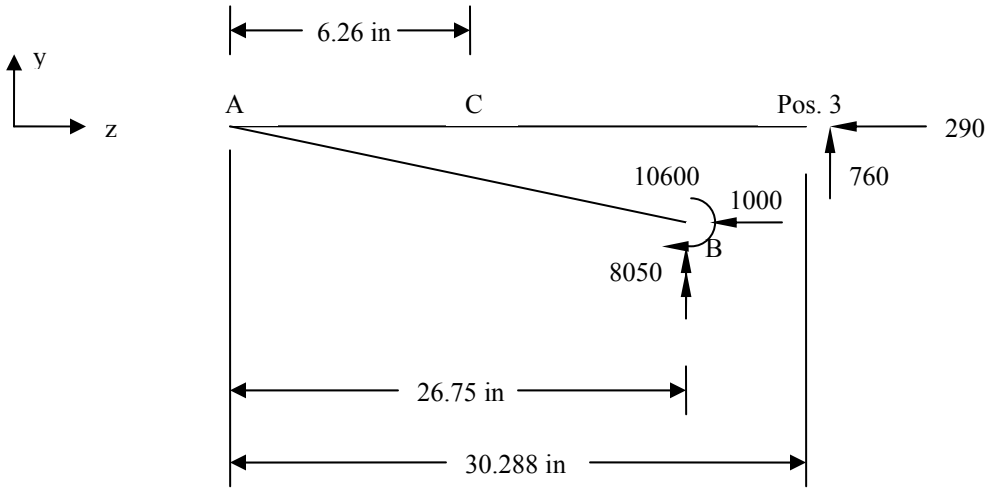

$D_o = 5.00\ in$
$D_i = 4.77\ in$

$A = 1.765 in^2$

$$I_{XX} = I_{YY} = \frac{\pi}{4}\left(r_o^4 - r_i^4\right) = 5.267 in^4$$

Resolve loads in Drag Beam Axes:
(loads in *lbs*)

$$F_{y-1000} = 1000\left(Sin\left(26^o 51'\right)\right) = 452$$
$$F_{z-1000} = 1000\left(Cos\left(26^o 51'\right)\right) = 892$$
$$T = 8050\left(Sin\left(26^o 51'\right)\right) = 3636$$
$$M_{xx} = 8050\left(Sin\left(26^o 51'\right)\right) = 7182$$

Determination of Internal Loads at section C:

$$F_Z = 892 + 290 = 1182 \rightarrow compression$$
$$T = 3636 \rightarrow tension$$
$$M_{XX} = 7182 \rightarrow tension$$
$$M_{YY} = -452(26.75 - 6.26) - 10600 + 706(30.288 - 6.26) = 2898 \rightarrow compression$$
$$M_{RES} = \sqrt{(M_{XX})^2 + (M_{YY})^2} = \sqrt{(7182)^2 + (2898)^2} = 7745$$

Appendix G – ANSYS FE Batch Command File for the Main Gear Drag Beam

```
/COM,ANSYS MEDIA REL. 9.0 (10/15/2004) REF. VERIF. MANUAL: REL. 9.0
/PREP7
smrt,off
/TITLE, Cylindrical Step Down Tube, Shell43, JMC
ANTYPE,STATIC
ET,1,SHELL43

R,,0.115                    ! Tube Thickness

MP,EX,1,27.0E6              ! Material Properties (1)
MP,NUXY,1,.33
MP,EX,2,27.0E6              ! Material Properties (2)
MP,NUXY,2,.33
MP,EX,3,27.0E6              ! Material Properties (3)
MP,NUXY,3,.33

CSYS,1

MW1=2.4425                  ! Midplane of smaller tube wall
K,1,MW1,0,0                 ! Inner Radius = 2.385, Outer Radius = 2.5
K,2,MW1,90,0                ! Midsurface = 2.4425
K,3,MW1,180,0
K,4,MW1,270,0
K,5,MW1,0,5
K,6,MW1,90,5
K,7,MW1,180,5
K,8,MW1,270,5
K,9,MW1,0,7
K,10,MW1,90,7
K,11,MW1,180,7
K,12,MW1,270,7
K,13,MW1,0,8
K,14,MW1,90,8
K,15,MW1,180,8
K,16,MW1,270,8

MW2=2.7                     ! Midplane of larger tube wall
K,17,MW2,0,8                ! Inner Radius = 2.6425, Outer Radius = 2.7575
K,18,MW2,90,8               ! Midsurface = 2.700
K,19,MW2,180,8
K,20,MW2,270,8
K,21,MW2,0,8.5
K,22,MW2,90,8.5
K,23,MW2,180,8.5
K,24,MW2,270,8.5
K,25,MW2,0,10.0
```

```
K,26,MW2,90,10.0
K,27,MW2,180,10.0
K,28,MW2,270,10.0
K,29,MW2,0,11.5
K,30,MW2,90,11.5
K,31,MW2,180,11.5
K,32,MW2,270,11.5

A,1,2,6,5                    ! Define Areas for first Tube
A,2,3,7,6
A,3,4,8,7
A,4,1,5,8
A,5,6,10,9
A,6,7,11,10
A,7,8,12,11
A,8,5,9,12
A,9,10,14,13
A,10,11,15,14
A,11,12,16,15
A,12,9,13,16

A,17,18,22,21                ! Define Areas for Second Tube
A,18,19,23,22
A,19,20,24,23
A,20,17,21,24
A,21,22,26,25
A,22,23,27,26
A,23,24,28,27
A,24,21,25,28
A,25,26,30,29
A,26,27,31,30
A,27,28,32,31
A,28,25,29,32

A,13,14,18,17                ! Construction of common wall between 2 tubes
A,14,15,19,18                ! Needed for Construction of fillet
A,15,16,20,19
A,16,13,17,20

AGLUE,1,2,3,4,5,6,7,8,9,10,11,12,13,14,15,16,17,18,19,20,21,22,23,24,25,26,27,28

AFILLT,9,25,0.25             ! Create area fillet with constant radius=0.25
AFILLT,10,26,0.25
AFILLT,11,27,0.25
AFILLT,12,28,0.25

NuDiv=20                     ! Define number of circumferential nodes per quarter circle
```

```
LESIZE,2,,,14                ! Define Divisions for first Tube
LESIZE,4,,,14
LESIZE,6,,,14                ! Specifies the divisions and spacing ratio on unmeshed lines
LESIZE,9,,,14
LESIZE,1,,,NuDiv
LESIZE,5,,,NuDiv
LESIZE,8,,,NuDiv
LESIZE,11,,,NuDiv
LESIZE,3,,,NuDiv
LESIZE,7,,,NuDiv
LESIZE,10,,,NuDiv
LESIZE,12,,,NuDiv

LESIZE,13,,,12
LESIZE,15,,,12
LESIZE,16,,,12
LESIZE,18,,,12
LESIZE,14,,,NuDiv
LESIZE,17,,,NuDiv
LESIZE,19,,,NuDiv
LESIZE,20,,,NuDiv

LESIZE,66,,,5
LESIZE,68,,,5
LESIZE,70,,,5
LESIZE,71,,,5
LESIZE,64,,,NuDiv
LESIZE,67,,,NuDiv
LESIZE,69,,,NuDiv
LESIZE,72,,,NuDiv

LESIZE,49,,,3                ! Define Divisions for Second Tube
LESIZE,51,,,3
LESIZE,52,,,3                ! Specifies the divisions and spacing ratio on unmeshed lines
LESIZE,54,,,3
LESIZE,50,,,NuDiv
LESIZE,53,,,NuDiv
LESIZE,55,,,NuDiv
LESIZE,56,,,NuDiv
LESIZE,42,,,NuDiv
LESIZE,45,,,NuDiv
LESIZE,47,,,NuDiv
LESIZE,48,,,NuDiv

LESIZE,41,,,5
LESIZE,43,,,5
LESIZE,44,,,5
LESIZE,46,,,5
```

```
LESIZE,31,,,NuDiv
LESIZE,35,,,NuDiv
LESIZE,38,,,NuDiv
LESIZE,40,,,NuDiv

LESIZE,30,,,5
LESIZE,32,,,5
LESIZE,34,,,5
LESIZE,37,,,5
LESIZE,29,,,NuDiv
LESIZE,33,,,NuDiv
LESIZE,36,,,NuDiv
LESIZE,39,,,NuDiv

LESIZE,22,,,6
LESIZE,23,,,6                    ! Division of fillet radius
LESIZE,57,,,6
LESIZE,58,,,6
LESIZE,65,,,NuDiv
LESIZE,75,,,NuDiv
LESIZE,80,,,NuDiv
LESIZE,82,,,NuDiv

LESIZE,76,,,1                    ! Division of small common wall
LESIZE,77,,,1
LESIZE,81,,,1
LESIZE,83,,,1

MAT,1
AMESH,1,4,1

MAT,2
AMESH,9,11,1
AMESH,29
AMESH,5,8,1
AMESH,13,16,1
AMESH,25,27,1
AMESH,30
AMESH,31,34,1

MAT,3
AMESH,17,20,1
AMESH,21,24,1
CSYS,0

!!!!!!!!!!!!!!!!!!!!!!!!!!!!!!!!!!!!!!!!!!!!!!!!!!!!!!!!!!!!!!!!!!!!!!!!!!!!!!!
!FOR FE-SAFE ANALYSIS
!Apply Internal Loadings              force=1182; torque=3636; moment=7745
```

```
nodeNUM=4*NuDiv                      ! Define number of circumferential nodes
forceZ=0.1526                        ! Define axial force
torqueZ=0.4695                       ! Define torque
momentX=1.0                          ! Define bending moment
momentY=1.0                          ! Define bending moment
!!!!!!!!!!!!!!!!!!!!!!!!!!!!!!!!!!!!!!!!!!!!!!!!!!!!!!!!!!!!!!!!!!!!!!!!!!!!!!!!!!!

NSEL,S,LOC,Z,11.5                    ! Define constraints on all nodes located at
D,ALL,UX,0                           ! z=10.5
D,ALL,UY,0
D,ALL,UZ,0
D,ALL,ROTX,0
D,ALL,ROTY,0
D,ALL,ROTZ,0

NSEL,ALL                             ! Unselect all nodes
NSEL,S,LOC,Z,0                       ! Define Applied Axial Force on nodes
F,ALL,FZ,forceZ/nodeNUM              ! Divide applied load by number of nodes
NSEL,ALL                             ! F=1.0 lbs in compression (positive sign)
NSEL,S,LOC,Z,0                       ! Define Applied Torque on nodes
F,ALL,MZ,-torqueZ/nodeNUM            ! Divide applied Torque by number of nodes
NSEL,ALL                             ! T=-1.0 in-lbs in tension (neg. sign)
NSEL,S,LOC,Z,0                       ! Define Bending Moment on nodes
F,ALL,MX,-momentX/nodeNUM            ! Divide applied Moment by number of nodes
NSEL,ALL                             ! Mx=-1.0 in-lbs in tension (neg. sign)
NSEL,S,LOC,Z,3.5,9.5                 ! Create a component or "group" within the
CM,CriticalSection,node              ! FE model from z = 3.5 to z = 9.5
alls
/VIEW,1,1,1,1
NSEL,S,LOC,Z,3.5,9.5
CM,CriticalSection-n,node
ESLN,S,1
CM,CriticalSection-e,elem
alls
CMGRP,CriticalSection,CriticalSection-n,CriticalSection-e

/SOLU
ANTYPE, STATIC
SOLVE
FINISH

/post1
SET,1
LCWRITE,1

CMSEL,S,CriticalSection              ! Plot nodal solution for
PLNSOL,S,Z                           ! Normal Stress Sigma_z
```

Appendix H – Load Definition File used for Main Gear Drag Beam

Detailed in this section is the LDF used to run the fatigue analysis simulation within fe-safe. The load history is given in Table 10.1 and consists of 26 constant amplitude blocks.

```
# Aircraft Load History
# Load History contains 26 Constant Amplitude Blocks
# SER-520081
#
# Actual Load History Values as seen in Table 10.1
#
INIT
Transitions=YES
END
#1
BLOCK n=190
ds=1, scale=18310
ds=1, scale=0
END
#2
BLOCK n=190
ds=1, scale=19566
ds=1, scale=0
END
#3
BLOCK n=190
ds=1, scale=56640
ds=1, scale=0
END
#4
BLOCK n=190
ds=1, scale=39960
ds=1, scale=0
END
#5
BLOCK n=150
ds=1, scale=25844
ds=1, scale=0
END
#6
BLOCK n=150
ds=1, scale=31604
```

ds=1, scale=0
END
#7
BLOCK n=150
ds=1, scale=86768
ds=1, scale=0
END
#8
BLOCK n=150
ds=1, scale=61214
ds=1, scale=0
END
#9
BLOCK n=35
ds=1, scale=34930
ds=1, scale=0
END
#10
BLOCK n=35
ds=1, scale=48830
ds=1, scale=0
END
#11
BLOCK n=35
ds=1, scale=127740
ds=1, scale=0
END
#12
BLOCK n=35
ds=1, scale=90122
ds=1, scale=0
END
#13
BLOCK n=2.5
ds=1, scale=43732
ds=1, scale=0
END
#14
BLOCK n=2.5
ds=1, scale=70496
ds=1, scale=0
END
#15
BLOCK n=2.5

ds=1, scale=175944
ds=1, scale=0
END
#16
BLOCK n=2.5
ds=1, scale=124130
ds=1, scale=0
END
#17
BLOCK n=140
ds=1, scale=5787
ds=1, scale=-1999
END
#18
BLOCK n=6
ds=1, scale=15520
ds=1, scale=-4498
END
#19
BLOCK n=1
ds=1, scale=29505
ds=1, scale=-8497
END
#20
BLOCK n=303
ds=1, scale=6787
ds=1, scale=-2999
END
#21
BLOCK n=13
ds=1, scale=17519
ds=1, scale=-6497
END
#22
BLOCK n=1
ds=1, scale=31004
ds=1, scale=-9996
END
#23
BLOCK n=23
ds=1, scale=6787
ds=1, scale=-2999
END
#24

```
BLOCK n=1
ds=1, scale=20018
ds=1, scale=-8996
END
#25
BLOCK n=1
ds=1, scale=7287
ds=1, scale=-3499
END
#26
BLOCK n=1
ds=1, scale=7287
ds=1, scale=-3499
END
```

Appendix I – Fe-safe Output File for Main Gear Drag Beam, t = 0.115 inches

Asking for module fe-safe/GUI - got 0
Asking for module fe-safe/Analysis - got 0
Asking for module fe-safe - got 1
Asking for module Database - got 1
Setting material to ASTM-A579-G72 in database C:\Program Files\fesafe\version.5.2\database\system.dbase
  Checking C:\Documents and Settings\Administrator\My Documents\fesafe.version.5.2\\local.dbase
  Checking C:\Program Files\fesafe\version.5.2\database\system.dbase
  Found database
    Checking AL1100-T6
    Checking AL2014-T6
    Checking AL2024-T351
    Checking AL2024-T4
    Checking AL5456-H311
    Checking AL7075-T6
    Checking BS1470-G5083
    Checking L119
    Checking BS1490-LM13
    Checking BS1490-LM16
    Checking BS1490-LM25
    Checking BS1490
    Checking BS1490-LM27
    Checking BS4360-G40B
    Checking BS4360-G43A
    Checking BS4360-G43C
    Checking BS4360-G43D
    Checking BS4360-G43D-2
    Checking BS970 G040A10
    Checking BS970 G53M40
    Checking BS970 G150M19
    Checking BS4360 G50A
    Checking BS970 G225M44
    Checking BS970 G605M36
    Checking BS970 G817M40
    Checking BS970 G835M40
    Checking ASTM-A514F
    Checking ASTM-A579-G71
    Checking ASTM-A579-G72
Material set OK.
No Strain Rates defined : Continuing without strain rate dependency ...

Reading LDF file C:\Program Files\fesafe\version.5.2\data\Drag_Beam_Load_History.ldf
INIT
Transitions=YES
END
BLOCK n=190
ds=1, scale=15454
ds=1, scale=0
END
BLOCK n=190
ds=1, scale=16514
ds=1, scale=0
END
BLOCK n=190
ds=1, scale=47805
ds=1, scale=0
END
BLOCK n=190
ds=1, scale=33727
ds=1, scale=0
END
BLOCK n=150
ds=1, scale=21815
ds=1, scale=0
END
BLOCK n=150
ds=1, scale=26674
ds=1, scale=0
END
BLOCK n=150
ds=1, scale=73234
ds=1, scale=0
END
BLOCK n=150
ds=1, scale=51666
ds=1, scale=0
END
BLOCK n=35
ds=1, scale=29482
ds=1, scale=0
END
BLOCK n=35
ds=1, scale=41213
ds=1, scale=0

END
BLOCK n=35
ds=1, scale=107815
ds=1, scale=0
END
BLOCK n=35
ds=1, scale=76065
ds=1, scale=0
END
BLOCK n=2.5
ds=1, scale=36911
ds=1, scale=0
END
BLOCK n=2.5
ds=1, scale=59500
ds=1, scale=0
END
BLOCK n=2.5
ds=1, scale=148500
ds=1, scale=0
END
BLOCK n=2.5
ds=1, scale=104768
ds=1, scale=0
END
BLOCK n=140
ds=1, scale=4885
ds=1, scale=-1687
END
BLOCK n=6
ds=1, scale=13099
ds=1, scale=-3797
END
BLOCK n=1
ds=1, scale=24903
ds=1, scale=-7171
END
BLOCK n=303
ds=1, scale=5729
ds=1, scale=-2531
END
BLOCK n=13
ds=1, scale=14786
ds=1, scale=-5484

END
BLOCK n=1
ds=1, scale=26168
ds=1, scale=-8436
END
BLOCK n=23
ds=1, scale=5729
ds=1, scale=-2531
END
BLOCK n=1
ds=1, scale=16895
ds=1, scale=-7593
END
BLOCK n=1
ds=1, scale=6151
ds=1, scale=-2953
END
BLOCK n=1
ds=1, scale=6151
ds=1, scale=-2953
END
End of read LDF file C:\Program Files\fesafe\version.5.2\data\Drag_Beam_Load_History.ldf

Starting Analysis ...
Asking for module fe-safe/Analysis - got 0
Asking for module fe-safe - got 1

FATIGUE LIFE : 5.2-00 fe-safe[mswin]

Copyright Safe Technology 1996-2006

Group Name Algorithm Material Surface-
KtFile Residual Kt UTS
Remainder Do not analyse
Material 2 BrownMiller:-Morrow ASTM-A579-G72-system.dbase
Mirror Polished - Ra <= 0.25 um-default.kt 1 270.051 ksi

Model File (s) C:\Program
Files\fesafe\version.5.2\data\Ansys\DB_115E_Refined_Norm.rst
FEA Units S=psi e=strain T=deg.C
Loading Loading is equivalent to 1 Repeats
Load Definition File : Drag_Beam_Load_History.ldf

Elastic FEA
Scale factor 1
Overflow Life value 0
Infinite Life value Material CAEL
Temperature analysis Enabled if temperatures present
Histories None
Log None
List of Items None,
Histories for Items None
Log for Items None
Output contours to C:\Documents and Settings\Administrator\My Documents\fesafe.version.5.2\Results\DB_115E_Refined_NormResults_9.rst
Contour variables LOGLife-Repeats,
....Intermediate C:\Documents and Settings\Administrator\My Documents\fesafe.version.5.2\Results\fesafe.fer
Influence coeffs. Disabled
Gauges. Disabled

D'set	Step	Inc	T/Freq	Type	Pos	Number	What	Direct
1	1	1	1.0	S	Elemental	4080	elements	101 -> -102

D'set	Shear	File	Description
1	68 -> -66	DB_115E_Refined_Norm.rst	Cylindrical Step Down Tube, Shell43, JMC

%	Time	Life-Repeats	
0	0:00:00	1325@3160.6	1 of 4080

Shear plane summary:
1-3 plane 0.0 %
2-3 plane 100.0 %
1-2 plane 0.0 %

Summary
=======
Worst Life-Repeats : 1324.742
at Element 3160.6
Analysis time : 0:00:00

Fatigue Analysis Completed.
Results exported by default (General FE Options)...
DLL mode ...

ansys_io.dll/.sl version 5.2-00

Interface to ANSYS .rst datafiles

Source file : C:\Program Files\fesafe\version.5.2\data\Ansys\DB_115E_Refined_Norm.rst
ANSYS Output : C:\Documents and Settings\Administrator\My Documents\fesafe.version.5.2\Results\DB_115E_Refined_NormResults_9.rst
Results File : C:\Documents and Settings\Administrator\My Documents\fesafe.version.5.2\Results\fesafe.fer
contains : LOGLife-Repeats
From ANSYS version : 9.0
Exporting set : 1
Variable : LOGLife-Repeats
as : Sx
Header updated, adding element data.
Results handler intelligent sorting 'CRESHND_SORT=2', there are too few items for a pre-sort to be beneficial
ANSYS writer (dll) completed
Time in module : 0:00:00

DLL mode done